Master of Science

Synthesis of morphology-controlled NiCu-electrocatalysts for efficient ammonia electrooxidation: Ni-Cu mutual cooperation mechanism

The Graduate School of University of Ulsan

School of Chemical Engineering

Vu Hoang Khoi

Master of Science

Synthesis of morphology-controlled NiCu-electrocatalysts for efficient ammonia electrooxidation: Ni-Cu mutual cooperation mechanism

The Graduate School of University of Ulsan

School of Chemical Engineering

Vu Hoang Khoi

Synthesis of morphology-controlled NiCu-electrocatalysts for efficient ammonia electrooxidation: Ni-Cu mutual cooperation mechanism

Supervisors: Professor Jin Suk Chung

A Dissertation

Submitted to

The Graduate School of the University of Ulsan

In partial Fulfillment of the Requirements for the Degree of

Master of Science in Chemical Engineering

by

Vu Hoang Khoi

School of Chemical Engineering

Ulsan, Korea

June 2023

Synthesis of morphology-controlled NiCu-electrocatalysts for efficient ammonia electrooxidation: Ni-Cu mutual cooperation mechanism

This certifies that the master's thesis

of Vu Hoang Khoi is approved.

_____

Committee Chair Prof. Lee Chan Hyun

_____

Committee Member Prof. Seung Hyun Hur

_____

Committee Member Prof. Jin Suk Chung

School of Chemical Engineering

Ulsan, Korea

June 2023

ACKNOWLEDGEMENTS

It was pure fate that brought me to Ulsan and let me thoroughly feel the taste of staying in a foreign city and apart from family and friends. Excitation and disappointment, enthusiasm and boredom, pride and nostalgia, happiness, and sorrow, I have tasted them all. Whether it was up or down, these experiences were truly invaluable to me, they equipped me with courage, determination, and gratitude to face and feel life with an open, warm but tough heart.

I want to express my deep appreciation to my advisor, Professor. Jin Suk Chung with all of his precious lessons and cares. He is as supportive a supervisor as I have ever known. Not only did he fulfill all of my financial necessities but also enthusiastically guided and equipped me with skills and knowledge for research.

I also want to say thanks to Dr. Tahereh, she was the only person who stood by me when I had trouble. She is truly a gift that God has brought to me. A caring mother, an enthusiastic lab mate, and a sincere friend are what I could describe her. Thank you very much from the bottom of my heart.

I would like to thank Dr. Sharma for all the valuable advice and good times that we have shared, thank Pragyan, Dang Thanh Truong, Vuong Hoai Thanh, and Nguyen Thi Kieu Oanh for their support and friendship during my working time. Thank Do Phuong Uyen for the care, understanding, and infinite encouragement that I have received from you.

Finally, I would like to express my deepest gratitude to my father and mother, who have always remotely encouraged me and provided invaluable orientation as well as a positive mindset. Without them, I would definitely not be able to achieve this far.

Thank you for not giving up, you are about to make it, Khoi – Kevin.

Ulsan, May 2023

Author

Vu Hoang Khoi.

ABSTRACT

Herein, facile synthesis of morphology-controlled NiCu-based electrocatalysts is presented using dodecylamine as a precipitation agent (NiCu-D). Several shapes, including scattering particles, spheres, and cubes, were created by adjusting the ratio of dodecylamine to metal precursor content. Compared with other precipitation agents, the optimized NiCu-D electrocatalyst exhibited a large electrochemically active surface area and an enhanced current density toward AOR. Cyclic voltammetry experiment found that NiCu-D-1:2/CP had a current density of 44.9 mA/cm^2 at 0.6 V vs. Hg/HgO.

In addition, we propose a new reaction pathway to explain the improvement in AOR reactivity after the addition of copper to the nickel system. This mechanism may explain how the two metals work together to lower the energy barrier, enhance reaction kinetics, and promote N_2 selectivity. Furthermore, the influences of Cu insertion into the Ni electrode and the electrode's active surface area were reflected in a substantial shift to N_2 selectivity up to 79 %, which was confirmed using an *in-operando* gas chromatography (GC) system. This study not only proposes a facile method of synthesizing well-defined hierarchical electrocatalysts with elevated AOR activity but also provides valuable insight into the mutual impacts of Ni and Cu in AOR, paving the way for the design of highly selective electrodes.

TABLE OF CONTENTS

LIST OF FIGURES

LIST OF TABLES

CHAPTER 1: INTRODUCTION

1.1. Ammonia

1.1.1. Physicochemical properties and uses

Ammonia is a colorless, pungent gas with the carbon-free molecular formula of NH_3. In nature, it can be found in trace amounts due to the metabolism of some animals and vegetables. NH_3 can be liquified at -33.1^oC in atmospheric pressure or 10.62 bara at 300K (Table 1.1), which is facile enough for long-term storage and international shipping [1]–[3]. In its atomic scale, NH_3 hybridizes in sp^3 type, which results in the arrangement of the four atoms to a trigonal pyramid shape with the H-N-H bond angle of 107^o (Figure 1.1). Since there is a leftover electron pair which can be donated, NH_3 has a characteristic of a Lewis base and is able to create coordination bonding with various metallic ions to form complexes.

NH_3 is a highly versatile compound that has been widely utilized in many applications, especially fertilizers. In fact, the world's agriculture has a strong connection to the development of NH_3. The artificial NH_3 production by Haber-Bosch process is believed to facilitate the Third Agricultural Evolution, leading to the increase in crop yields of 44 % from 1965 to 2010. Surprisingly, 50 % of N content of all agricultural products in the world nowadays is supplied by synthetic NH_3. And to fulfill the global food demand, 150 million ton of NH_3 has been synthesized in 2023, which is 1.5 time greater than that in 2001 and 100 time than in 1945 (Figure 1.2) [4]. The infrastructure required for NH_3 storage and distribution

are therefore advanced accordingly, paving the way for the development in many other fields. Ammonia is utilized all over the world, not just in the fertilizer sector, but also as a precursor in the production of commercial explosives, chemical substances, and other products. Other minor applications include cleaning solutions for household appliances [5]–[8].

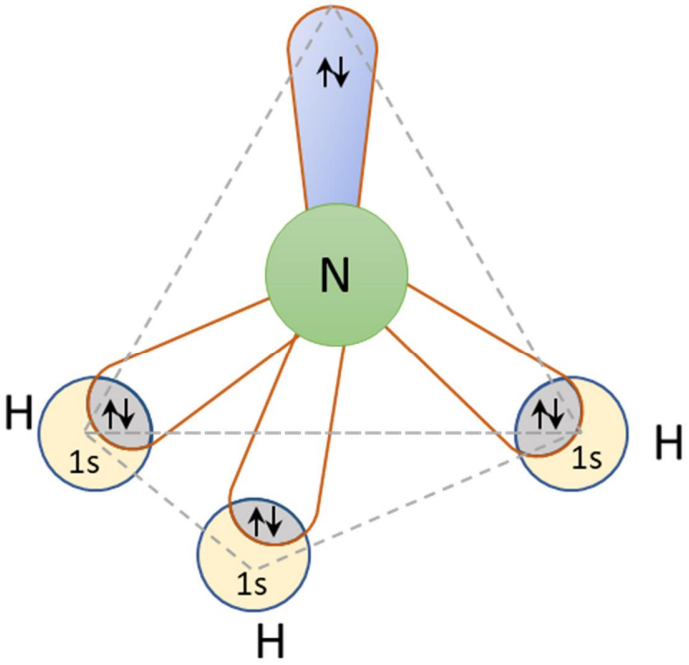

Figure 1.1. Molecular structure of NH_3

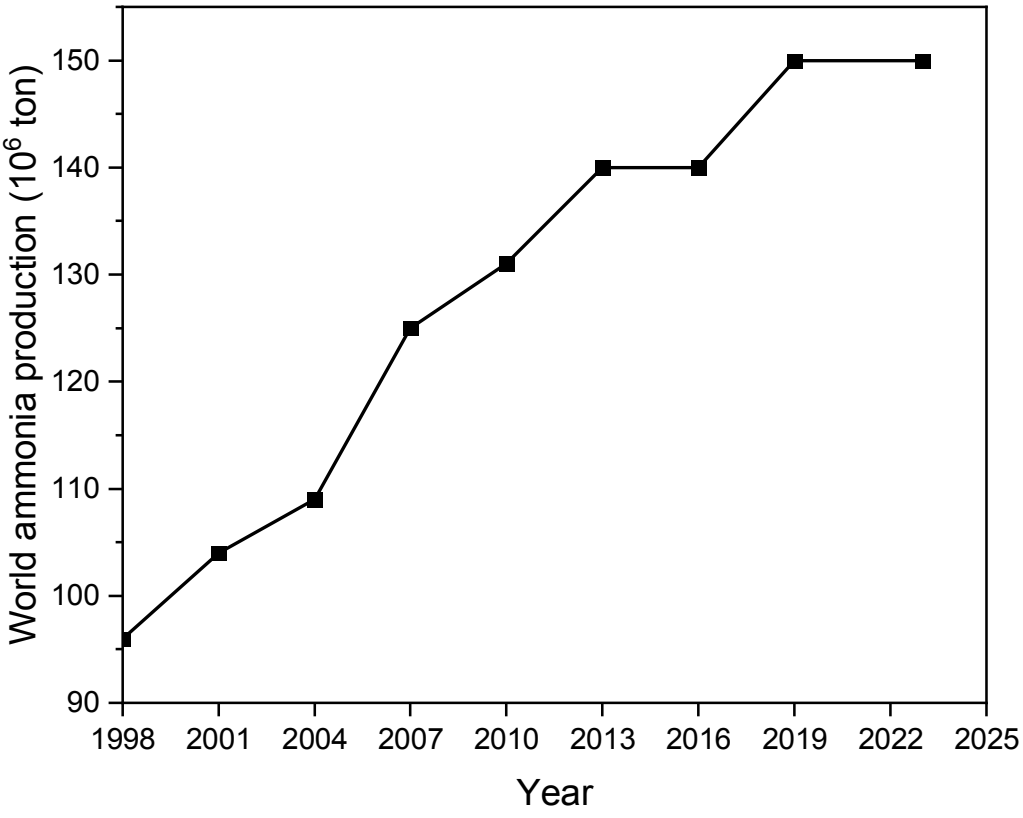

Figure 1.2. The growth of global NH_3 production from 1998 to 2023 (ammonia production unit: megaton)

1.1.2. Applications in energy field

Aside from the above-mentioned applications, NH_3 is arising as a renewable energy carrier that can solve the energy crisis problem. NH_3 structure contains three hydrogen atom covalently bonding to a N atom, therefore, the NH_3 shows a high hydrogen-content of 17.6 % m/m. In addition, the N-H bonding has the medium energy of 391 kJ/mol, making NH_3 a perfect candidate for energy-relating applications. The facile liquification of NH_3 enables cost-efficient transportation and storage. Practically, the liquefied NH_3 at -33.1^oC possesses an energy density of 12.7MJ/L, in comparison to 8.5 MJ/L of liquid hydrogen at approximately -250^oC [5], [6]. It should be noted that extra precautions should be paid since NH_3 is highly hazardous and explosive. However, the specialized equipment, infrastructure, and regulations for handling ammonia that have been built over a hundred years are sufficient to control this compound.

In an effort to achieve "zero-carbon emission" in 2050, scientists and engineers are highlighting the importance of NH_3 as the key intermediate for sustainable energy conversion, transportation, and storage. The zero-carbon ammonia technological roadmap includes three main steps: production, storage & transport, and utilization. Therein, Green ammonia is first produced from green hydrogen synthesized by sea water electrolyzer, then transported internationally by mainly maritime routes or pipe systems and stored under an appropriate pressure. For the utilization step, NH_3 can be converted into other forms of energy like H_2, electricity, or heat by appropriate conversions. These include thermal reforming,

electrochemical oxidation, direct fuel cell, or fuel for combustion engines. Due to the carbon free structure of NH_3, the by-products contain only environmentally friendly N_2 gas and/or water vapor, guaranteeing the ecological sustainment of the process.

- **Production of NH_3**

Before the start of World War I, ammonia was mostly extracted from plantation and animal products by the dry distillation process. However, the yield was fairly small compared with industrial manufacturing. After the war, the Haber process became the main production source of NH_3 [9], [10]. The process utilizes a Fe-based catalyst with high temperatures to break the stubborn N≡N bonds, then it is allowed to react with hydrogen via an overall reaction:

$$N_2 + 3H_2 \rightarrow 2NH_3 \qquad \Delta H^0 = -91.8 \text{ kJ/mol} \qquad (1)$$

The world's NH_3 production would be much less without the Haber process. Scientists claimed that the introduction of the Haber process initialized the Green Evolution and the global population explosion in XX – XXI centuries. However, it is also considered as the "dirtiest process" from an environmental standpoint. Globally, Haber-Bosch consumes 2 % of the total world energy supply and is responsible for 450 million tons of CO_2 in 2010. The process relies heavily on fossil fuel to generate the required heat. Therefore, scientists and engineers are shifting their focus on a newer and greener method that utilizes an electricity current to produce NH_3 from N_2 and H_2 generated from water, so called electrochemical synthesis of NH_3 [11]–[16]. Extensive studies found that this process has the potential to unravel an era of sustainable energy, where the power is created and consumed without any

CO_2 emission. The ammonia energy cycle is gaining international traction, numerous funds and projects relating to this topic have been signed from 2018, ranging across continents.

- **Utilization of NH_3**

As mentioned above, NH_3, after reaching the desired destination, can be converted into various forms for uses. Because the hydrogen fuel cell has been well developed and commercialized, the conversion of NH_3 to hydrogen for further uses is necessary. In the framework of this thesis, only the oxidation processes of NH_3 to generate hydrogen are discussed, which includes thermal oxidation and electrochemical oxidation reactions. In thermal oxidation reaction, NH_3 is decomposed to N_2 and H_2 gases with the help of specialized catalysts under high temperature. This process has drawn scientific attention thanks to its simplicity and feasibility of upscale. However, as the cracking reaction is highly endothermic, it is necessary to use an external heat supplier from coal to maintain the appropriate condition, which makes the whole production line become a "gray process". In addition, a complicated and energy-consuming separation process is required to obtain pure hydrogen from the mixed product stream, raising the total production cost [17]–[21].

Table 1.1. Properties of NH_3 and H_2

	NH_3	H_2
Molar mass	17 g/mol	2 g/mol
Melting point	-77.73 ^oC	-259.1 ^oC
Boiling point	-33.34 ^oC	-252.9 ^oC
Density (standard condition)	0.77 kg/m^3	0.09 kg/m^3
Solubility in water	31% w/w (25 ^oC)	-
Energy density	12.7 MJ/L	8.5 MJ/L

1.2. Ammonia electrochemical oxidation reaction

To overcome the mentioned drawbacks of the cracking method, NH_3 electrochemical oxidation reaction (AOR) has been taken into consideration. In a typical reactor, a DC voltage is applied to a system contains 2 electrodes dipped in electrolyte solution. The solution can either contain liquid NH_3, aqueous NH_3, or NH_3 dispersed in organic solvent. Usually, an amide compound such as NH_4NH_2, $NaNH_2$, KNH_2 is also added to liquid NH_3 or organic solvent for conduction of charged species. On the surface of anode, NH_3 oxidation reaction occurs and release dinitrogen N_2 gas while in cathode, reduction reaction takes place to form highly pure H_2 under the overall conversion:

$$2NH_3 \rightarrow N_2 + 3H_2 \qquad (X)$$

Compared with thermal decomposition, AOR can produce greener H_2 under a much more facile condition [8], [22]–[24]. The reaction is conducted at room temperature, and the products gases are produced on different electrodes, which significantly reduce the cost of operation and separation. In addition, the study of AOR simultaneously facilitates the development of direct fuel cell, NH_3 sensor, and hydrogen production from NH_3, since both share a similar concept. When combined, NH_3 production and AOR create a true net-zero-carbon energy cycle that is promising for the development of a sustainable world. Considering the drawback of this reaction, the only problem is regarding the catalysts used for oxidation

of NH_3 on anode. AOR suffers from sluggish kinetics and a low stability of catalytic materials. Studies revealed that a decent adsorptive strength is required for the reaction, as the molecule should be adsorbed and the three hydrogen atoms in NH_3 structure should be eventually removed. Unfortunately, over adsorption leads to difficulty in desorption of final products, then poisoning the catalytic surface. Therefore, either too low or too high NH_3 affinity of catalysts would drastically decrease the performance. Numerous experimental and theoretical studies were performed to give insights for proper AOR materials. And the understanding toward mechanism of this reaction is highly in demand for designing a robust electrocatalyst.

To date, there are two mechanisms that have been generally accepted to describe the AOR pathway in aqueous NH_3: the Gerischer–Maueuer (G-M) [2]and Oswin–Salomon (O-S) [25]mechanisms, as shown in Scheme 1 and Scheme 2, respectively. For both routes, NH_3 is first adsorbed on the catalytic surface and subsequently oxidized to NH_2* (2) and NH* (3). Next, in the G-M mechanism, two arbitrary species can combine to form N_2H_{x+y}* (4), which is then deprotonated to N_2* (5). In the O-S mechanism, an N* adatom is formed from the oxidation of NH* (6), and the dimerization step occurs with two N* (7).

Table 1.2. Gerischer–Maueuer (G-M) mechanism of the AOR process

Gerischer–Maueuer mechanism	
$NH_3 \rightarrow NH_3^*$	(1)
$NH_3^* + OH^- \rightarrow NH_2^* + H_2O + e^-$	(2)
$NH_2^* + OH^- \rightarrow NH^* + H_2O + e^-$	(3)
$NH_x^* + NH_y^* \rightarrow N_2H_{x+y}^*$	(4)
$N_2H_{x+y}^* + (x + y)\ OH^- \rightarrow N_2^* + (x + y)\ H_2O + (x + y)\ e^-$	(5)

Here * denotes species adsorbed on a catalytic surface.

Table 1.3. Oswin–Salomon (O-S) mechanism of the AOR process

Oswin–Salomon mechanism	
$NH_3 \rightarrow NH_3^*$	(1)
$NH_3^* + OH^- \rightarrow NH_2^* + H_2O + e^-$	(2)
$NH_2^* + OH^- \rightarrow NH^* + H_2O + e^-$	(3)
$NH^* + OH^- \rightarrow N^* + H_2O + e^-$	(6)
$N^* + N^* \rightarrow N_2^*$	(7)

Density functional theory (DFT) has proven that G-M mechanism is more favorable at low applied potential, as it suggests a lower onset potential than O-S pathway [26]–[30]. However, the G-M is constrained by the sluggish dimerization (Equation (4)), which is not affected by the applied potential. Therefore, experiments showed that under high voltage, the O-S mechanism dominates and controls the results, which includes the response current and the selectivity of final products.

Aside from the activity, the selectivity of the final products plays an important role in catalytic application. In aqueous solution, NH_3 can be oxidized into both inert N_2 gas, or oxygenated NO_2^- and NO_3^- (here denoted as NO_x). Since NO_x is highly toxic, the high selectivity toward N_2 guarantees a safer environmental impact of the process and eliminates the cost of treatments. Recent studies have found that the N* species is the precursor of NO_x formation at high applied voltage. With its high adsorption strength on catalytic surface, two adjacent N* are not likely to dimerize to form dinitrogen but are further oxidized to NO_x ions. According to the mechanisms above, G-M pathway promotes higher N_2 selectivity since N* is not formed during the process. DFT calculations have found that the dimerization is the slowest step in G-M route, while the formation of N* (Eq – 6) is the rate-determining step of O-S [27], [31], [32]. Therefore, the ease in dimerization promotes the reaction follow G-M pathway, which favors the N_2 selectivity.

Another condition that effectively alters the selectivity of AOR is the coverage of reactive species, i.e., NH_2*, NH*, as it directly affects the feasibility of dimerization. For the formation

of one dimerized N_2H_{x+y} species, two adjacent arbitrary NH_x* and NH_y* are required rather than a single one. Meanwhile, the probability of the two species being adjacent is proportional to the square of the electrochemical active surface area, $ECSA^2$. As a result, the increase in ECSA significantly enhances the rate of the dimerization step and turns the reaction towards the G-M pathway.

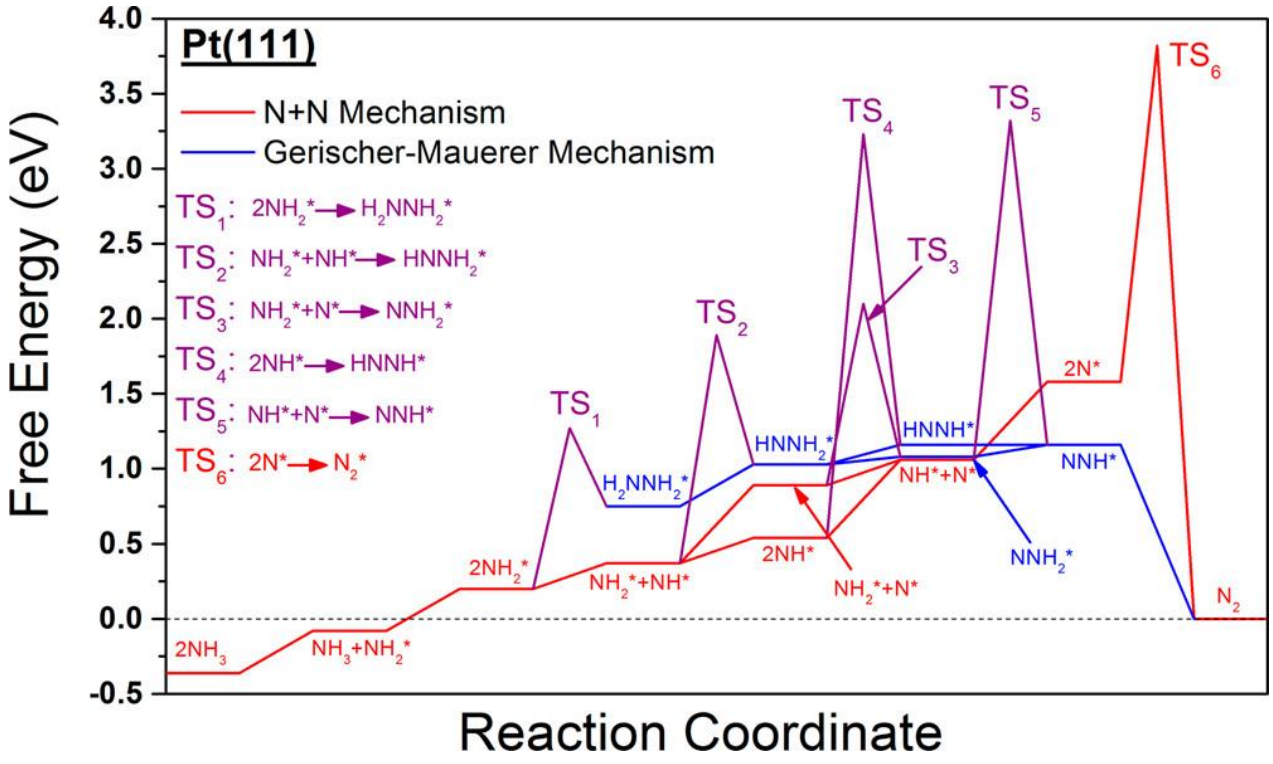
Pt(111)
N+N Mechanism
Gerischer-Mauerer Mechanism
TS1: 2NH2*→H2NNH2*
TS2: NH2*+NH*→HNNH2*
TS3: NH2*+N*→NNH2*
TS4: 2NH*→HNNH*
TS5: NH*+N*→NNH*
TS6: 2N*→N2*
Free Energy (eV)
Reaction Coordinate
4.0
3.5
3.0
2.5
2.0
1.5
1.0
0.5
0.0
-0.5
2NH3
NH3+NH2*
2NH2*
TS1
H2NNH2*
NH2*+NH*
TS2
HNNH2*
2NH*
TS3
NH2*+N*
TS4
HNNH*
NH*+N*
TS5
NNH2*
2N*
NNH*
TS6
N2

1.2.1. Noble metal based materials

Which metal is optimal for ammonia oxidation has been the subject of extensive investigation. Pt is still the most effective metal for enhancing the kinetics of the ammonia electro-oxidation process, despite its high cost. The high activity of this metal comes from the appropriate adsorption strength of ammonia. Either stronger or weaker strength lead to the deactivation of the material. Aside from Pt, precious transition metals (Pt, Pd, Rh, Ru, and Ir) as well as coinage metals (Cu, Ag, and Au) have been extensively studied for AOR application. Both calculational and experimental results found that the affinity of NH_3 on metallic surface are ordered as Ru > Rh > Pd > Ir > Pt >> Au, Ag, Cu. Aside from Pt, other metals showed inactiveness toward ammonia oxidation. On Ru, Rh, Pd, and Ir surface, the over adsorption occurred that lead to the formation of poisonous N* species that deactivate the reaction. Cyclic voltametric results of Ir showed a lower onset potential as compared to Pt, however, the intensity was much less than that of Pt, implying that surface has been deactivated. Meanwhile, the weak interaction of coinage metals such as Cu, Ag, and Au is insufficient for dehydrogenation of NH_3, as a result, no activity was found from these materials.

Several efforts have been made to enhance the catalytic performance of Pt, which includes producing binary, ternary electrocatalysts, doping, surface modification, activation, etc. In general, these modification can alter the NH_3 – metallic surface interaction, increase the conductivity of materials, or reconfigure the electronic structure of Pt (d-band structure). Among the reported developments, Ru and Ir are the most chosen candidate for alloying or

doping with Pt, owing to their ability to boost up AOR performance of Pt. However, their synergistic effects were complicated and under controversy.

Electrocatalyst	Preparation method	Noble metal loading	Test protocol	Performance	Ref
Pt-Ir/Au	Potentiostatic electrodeposition	-	CV in 2-50 mM NH_3 + 0.1 M KOH solution	0.25 mA/cm^2	[33]
Pt-M alloys/CP	Potentiostatic electrodeposition	20 mg/cm^2	CV in 5M KOH	130 mA/cm^2	[34]
Pt/Ni	Galvanostatic electrodeposition	2 mg/cm^2	CV in 0.1 M NH_3 + 1 M KOH	1 mA/cm^2	[35]
Pt/C	Modified polyol method	20 wt% of metal loading	CV in 0.5 M NH_3 + 1M KOH	6 mA/cm^2	[36]

Pt-M/C (M = Pd/Ir)	Modified polyol method	20 wt% of metal loading	CV in 0.5 M NH_3 + 1 M KOH	4 mA/cm^2	[36]
Pt-Pd-Rh/Glassy carbon	Coprecipitation method	-	CV in 0.1 M NH_3 + 0.5 M H_2SO_4	0.3 mA/cm^2	[37]

1.2.2. Non-noble metal based materials

As a common knowledge, the high cost of noble metal electrocatalysts prevent them from commercial uses. Any noble metal content excesses 20 mg/cm^2 is considered impractical for up-scaling, therefore, the studies of non-noble transition metals are in high demand. Unfortunately, they are generally incomparable to noble metal in terms of AOR activity. Their NH_3 affinities are either too strong (Ni, Co, Fe) or too weak (Cu, Zn) to give a satisfactory performance. Among the pure transition metals, Ni is the most studied candidate, owning to its activeness toward AOR. DFT calculations showed that Ni has the most similar energy bands of adsorbed intermediates to Pt, which might explain its activity. In situ studies of AOR

on Ni have shown that the active sites for AOR is oxyhydroxide species Ni(III)OOH, which is formed as a thin protection layer on the surface of Ni. Extensive studies have found that Ni compounds such as NiO or $Ni(OH)_2$ promote higher response current densities than that of metallic one, as NiOOH could be more facially generated from Ni(II) materials than Ni(0). However, the current density of Ni-based materials were relatively small and negotiated compared to Pt-based electrocatalysts.

Electrocatalyst	Test conditions	Current density	Ref
Ni	1 M $(NH_4)_2SO_4$ + 1 M KOH	0.1 mA/cm^2	[38]
$Ni/Ni(OH)_2$	150 mM NH_4ClO_4 + 1M $NaClO_4$ + NaOH (pH 9)	3.5 mA/cm^2	[39]
Ni sheets	1000 ppm $(NH_4)_2SO_4$ + 1M NaOH (pH 9.4)	0.5 mA/cm^2	[40]
Ni/C	0.055 M NH_4Cl + 0.5 M NaOH	-	[41]
$Ni(OH)_2$/Ni foam	0.1 M Na_2SO_4 + 0.003 M NH_3	2.7 mA/cm^2	[42]

1.2.3. NiCu based materials

It was not until the discovery of NiCu alloy in 2018 by Xu et al. that the AOR activity of Ni was incomparable to Pt-based materials. The researching group found that the introduction of Cu into Ni electrocatalysts could significantly enhance the AOR activity, while the combination of Ni and other metals (Zn, Mn, Fe, Co, etc.) does not promote any changes. The finding was then rapidly recognized and confirmed by various studies later, under different forms such as NiCu double layer, oxides, sulfides, etc. The enhancement in electrochemical activity is widely accepted, however, how Cu can improve the activity of Ni still remains unclear.

A research group of Jinping Jia was the first to identify the role of Cu site in Ni-Cu hydroxide electrocatalysts by using EIS and *in situ* FTIR. They concluded that on $Cu(OH)_2$ surface, NH_3 was fully dehydrogenated to form N*, which then either further oxidized to nitrite or dimerized to form N_2 gas. This mechanism is completely different from that on NiOOH, where the dimerization step of two arbitrary NH_x and NH_y takes place. However, the proposal was just based on qualitative characterization, and the authors did not elucidate how the Ni-Cu combination could improve the reaction rate. Zucheng Wu et al. revealed the d-band optimization for AOR when Cu is introduced to Ni by using both density functional theory (DFT) calculations and experimental tests. The appropriate modulation of the electronic configuration reduces the energy barrier of the reactions, thus speeding the reaction rate up. Nevertheless, only the mechanism towards the formation of N* was investigated,

while the dimerization to form N_2H_x* was omitted. Therefore, the suggested mechanism might not be the lowest-energy route for the reaction and might not describe the actual mechanism. Moreover, the high selectivity towards N_2 over NO_x of the catalyst after Cu introduction was not proven by practical experiments. Therefore, the interaction and synergistic effects between Cu and Ni should be extensively studied to provide such informative knowledge about AOR.

Considering the intrinsic drawbacks of each metal in its pure form, it is generally accepted that Ni has a great NH_x adsorption strength, which makes the dimerization process and products desorption more difficult. On the other hand, Cu creates weak bonds to NH_x that insufficient to conduct proper deprotonation, in return, Cu effectively promote dimerization, and the product can easily desorb from its surfac. These concepts were confirmed largely from both experimental and theoretical analyses. From this point of view, we inferred that Ni and Cu might undertake different tasks in the NH_3 oxidation reaction chains, which can lower activation barrier and improve the kinetic. Another factor that dramatically affect AOR performance is the adsorbate coverage on the surface of the adsorbent [13]. A High coverage of NH_2* was reported to aid the dimerization process to form N_2H_4* and raise the catalytic activity. Note that an elevated adsorbate coverage could be achieved by increasing the number of active sites of the electrode and/or having more surface exposed, therefore, structural and morphological control is crucial for enhancing electrochemical performance and selectivity. One approach that can fulfill this demand is synthesis of hierarchically structured

electrocatalyst, whose morphology is highly controlled to obtain the optimal adsorption of reactants, active surface area, and mass transfer properties [43]–[48].

1.3. Research objectives

As review above, the understanding of Ni and Cu mutual effects is of great importance to enable synthesis of robust AOR electrocatalysts in the future. To fulfill that requirement, the objectives of this thesis are:

- Synthesis of highly active electrocatalysts for AOR.
- Investigation of the effects of various precipitation agents on catalytic activity.
- Studying the impacts of dodecylamine content on AOR performance.
- Giving the explanation of how Cu introduction to Ni can significantly enhance the activity of materials.
- Studying the consequences of Cu introduction to Ni in AOR application.

CHAPTER 2: EXPERIMENTS

2.1. Materials

Nickel (II) acetate tetrahydrate ($Ni(OAc)_2.4H_2O$, 98 %), Copper acetate ($Cu(OAc)_2$, 98 %), Ammonium hydroxide (NH_4OH, 28 %), Triethylamine (TEA, 99 %), Dodecylamine (99 %), and 5 % Nafion^{TM}117 solution were purchased from Sigma-Aldrich. Sodium hydroxide (NaOH), and Nessler's Reagent were purchased from Samchun, South Korea. Ethanol, Hexane, and Ammonium chloride (NH_4Cl, 99 %) were bought from Daejung, South Korea. All chemicals were all analytical reagents and utilized without further purification. Carbon paper (CP, 0.3 mm thickness, 0.78 g/cm^3) was purchased from Wizmac.

2.2. Preparation methods

Morphology–controlled NiCu-D electrocatalysts were synthesized via a facile one-step solvothermal method. In brief, 0.5 mmol $Ni(OAc)_2.4H_2O$ and 0.5 mmol $Cu(OAc)_2$ were homogeneously dispersed in 80mL solvent of hexane and ethanol ($V_{hexane}/V_{ethanol}$ = 3/1). Subsequently, different moles of dodecylamine were quickly added to the above solution, causing the color to change from green to deep blue. After 5 min of stirring, the whole solution was transferred into a 100 mL Teflon-lined stainless steel autoclave, where it was then heated at 180^{o}C for 12 h. The resulted precipitation was put into vacuum filtration for washing and collecting. Warm ethanol at temperatures over 35^{o}C was used to wash the materials in order to thoroughly eliminate the dodecylamine residue on the catalysts. The electrocatalysts were

named NiCu-D-1:1, NiCu-D-1:2, and NiCu-D-1:4, corresponding to the initial additions of 1, 2, and 4 mmol of dodecylamine, respectively. Ni-D-1:2 was synthesized using a similar technique, except that 1 mmol Ni(OAc)2.4H2O was used instead of a mixture of Ni and Cu salts.

We also investigated the effects of different precipitation agents on the activity of the catalysts. The obtained samples were named NiCu-X (X = Urea, NaOH, NH_3, and TEA, respectively), which were produced via a similar process as NiCu-D-1:2, except the use of different precipitants in lieu of dodecylamine, and the polarized solvent was used by replacing hexane with water.

Carbon paper electrodes for each catalyst were prepared by drop-casting method prior to electrochemical experiments. A catalyst ink was prepared by homogeneously dispersing 4mg catalyst to 1mL water and 1ml isopropanol mixture with the addition of 20 μL Nafion^{TM}117 solution. The whole mixture was then put into an ultrasonicate bath for 20 min. Subsequently, 200 μL of catalyst ink was drop-casted onto 1 cm × 1 cm treated CP and dried under IR illumination for 1 hour before electrochemical measurements. The obtained electrode was named as NiCu-X/CP.

2.3. Characterization

An inductively coupled plasma atomic emission spectrometer (ICP-OES, 5110 VDV – Agilent Technologies) was used for quantifying the Ni and Cu contents in synthesized

materials. X-ray diffraction analysis (XRD) (Ultima 4 – Rigaku with $CuK_{\alpha 1}$ radiation) was applied for crystalline structure analysis of the materials. The morphologies and particle arrangement of catalysts were investigated using a scanning electron microscope (SEM, AIS2000C). Fourier transform infrared spectroscopy (FTIR, Nicolet iS5 – ThermoFisher SCIENTIFIC) was utilized for determining bonding compositions of synthesized materials. UV-Visible spectrophotometer (Specord@210 Plus – Analytikjena) was used for collecting absorbance data of Nesslerized solutions at 420 nm.

All electrochemical characterization proceeded in a three-electrode system, where coated CP was the working electrode, graphite rod was utilized as the counter electrode and Hg/HgO as the reference electrode. Prior to the tests, the working electrodes were electrochemically activated by employing cyclic voltammetry (CV) between 0 V and 0.8 V at the scan rate of 50 mV/s (vs Hg/HgO) for 100 scans in NaOH 0.5 M media. CV was recorded between 0 V and 0.8 V with a scan rate of 25 mV/s for 5 times. Linear sweep voltammetry (LSV) was recorded from 0 V to 0.8 V (vs Hg/HgO) with a scan rate of 2 mV/s. Electrochemical Impedance Spectrometry (EIS) was conducted from 10mHz to 100 kHz under 0.6 V (vs Hg/HgO). The electrolyte used for the above experiments was a mixture of NaOH 0.5 M and NH_4Cl 0.055 M. Double layer capacitance (C_{dl}) was measured by CV scanning in different scan rates between 0.3 to 0.4 V (vs Hg/HgO) where there was no Faradaic reaction, but the charging of double layer capacitor took place. The values of current density were chosen at the middle of the surveyed range (0.35 V). If there is no specific note, a solution

containing NaOH 0.5 M and NH_4Cl 0.055 M was used as the electrolyte for the above experiments.

2.4. Electrochemical activity tests

2.4.1. Ammonia removal test

The three-electrode system was used to quantify the ammonia removability of the electrocatalysts. The experiment was carried out in a 50 mL cylindrical electrochemical cell containing 30 mL of NaOH 0.5 M and NH_4Cl 0.05 M. A constant voltage of 0.6 V (vs Hg/HgO) was applied to the cell for 9 hours continuously. After each time interval, 10 μL of the electrolyte was taken out and added into 4.8mL of distilled water and shaken properly. Then 200 μL of Nessler's Reagent was injected dropwise under mild sonicating treatment for 10 minutes to obtain a transparent yellow solution. The absorbance of the solution was determined using a UV-Visible spectrometer at a wavelength of 420 nm. Note that sonication during Nessler's Reagent injection is crucial to obtain a well-transparent solution unless which, turbidity would occur and affect the results [49]. The calibration curve was built based on a similar protocol with the use of 0, 2, 4, 6, 8, and 10 μL standard NH_4Cl 0.05 M solution.

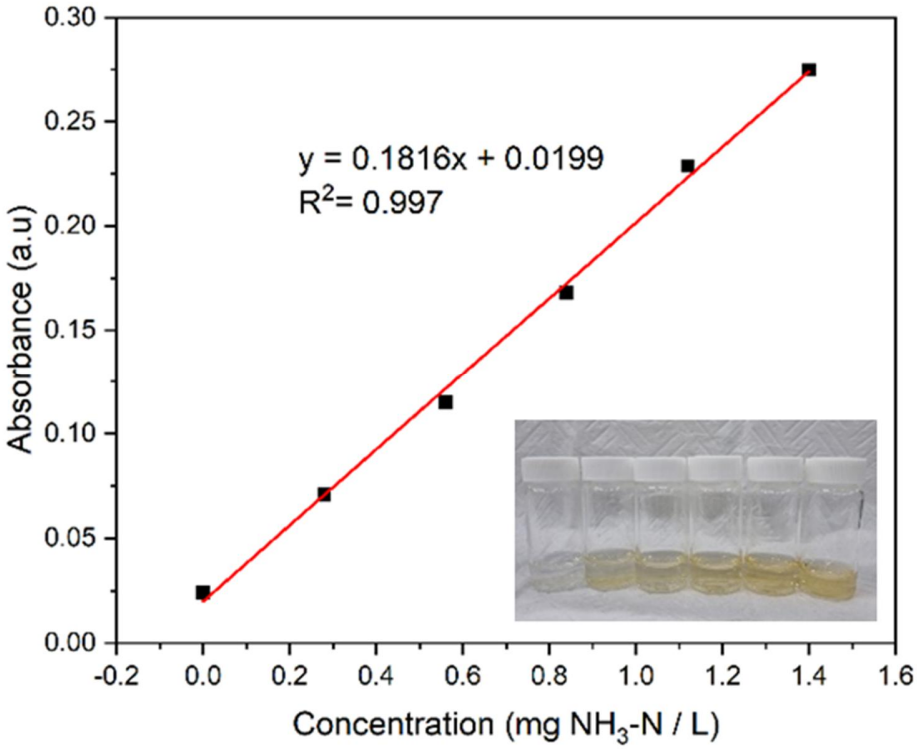

Figure 2.1. Calibration curve of Nessler's reagent

2.4.2. Gas measurement and Faradaic efficiency calculation

Gas chromatography (Agilent 8890 GC, 60/80 Carboxen 1000) was used for determining the gas produced from the analysis reaction. As the product stream contains a high amount of hazardous NH_3 evaporating from the electrolyte, it is necessary to completely remove NH_3 using a series of acid, water, and cold traps. Plus, a vacuum pump is required for the evacuation of N_2 and O_2 gases from the atmosphere. A diagram of the system for the gas measurement experiment is shown in Figure 2.2Figure 2.2. GC-TCD system for N2 and O2 quantification.. The experiment was conducted under the following steps: An air-tight electrochemical cell containing 30 mL 0.5 M NaOH and 0.05 M NH_4Cl electrolyte was connected to the system. The air inside the system was evacuated by vacuuming and then purging with 100 sccm Ar gas for 1 hour until no peak of N_2 and O_2 was observed from the GC spectra. Then, the flow rate of the carrier gas was adjusted to 15 sscm and a potential of 0.6 V vs Hg/HgO was applied to conduct the reaction. 250 μL of the product stream was automatically collected to the GC every 30 min interval. The concentrations of N_2 and O_2 were calculated via the positive correlation between the peaks' area and gas stream concentration, with the use of a calibration curve.

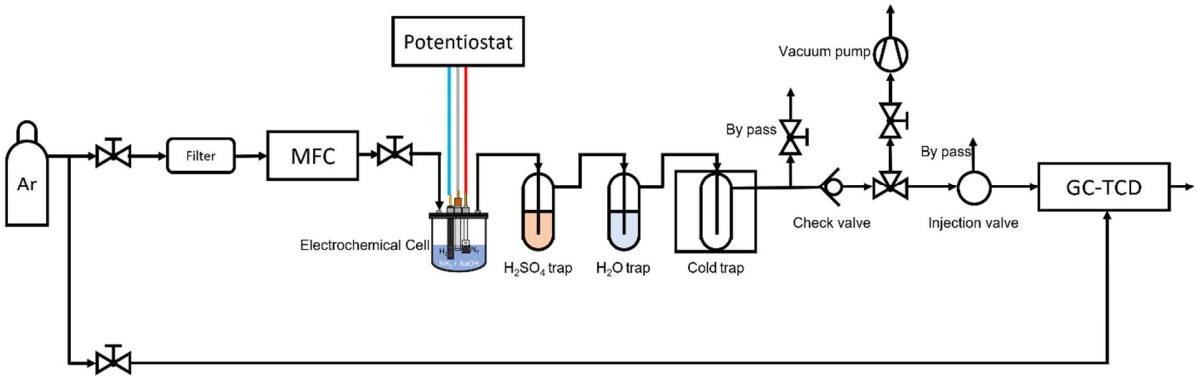

Figure 2.2. GC-TCD system for N_2 and O_2 quantification.

CHAPTER 3: RESULTS AND DISCUSSION

3.1. Preparation and characterization of NiCu-D electrocatalysts

The morphology-controlled NiCu-D electrocatalysts were synthesized via a simple one-step solvothermal method, as shown in Schematic Figure (Figure 3.1). In the precursor solution, dodecylamine acts as not only a precipitation agent but also a surfactant, which simultaneously enabled the growth and surface modification of catalysts. On the one hand, the metallic ions in the solution formed stable complexes with amine heads of dodecylamine (Equation (8)), creating an electron-rich and hydrophilic region. The long lipophilic hydrocarbon tail, on the other hand, interacts with the non-polarized hexane-ethanol solvent, leading to the formation of a micro reverse-micelle structure that serves as the predecessor for the final products. Consequently, the molar ratio of metal ions to dodecylamine (M:D) has a pivotal effect on regulating catalyst morphologies. First, starting with NiCu-D-1:1, the FE-SEM images (Figure 3.2(a) to (f)) showed micro-size blocks with unspecified structures. It is because the amount of dodecylamine in this sample is insufficient to promote a well-ordered assembly. Meanwhile, when a double dosage of dodecylamine was added, the catalyst morphology turned to unique spherical granules, which were built up by numerous agglomerated small particles.

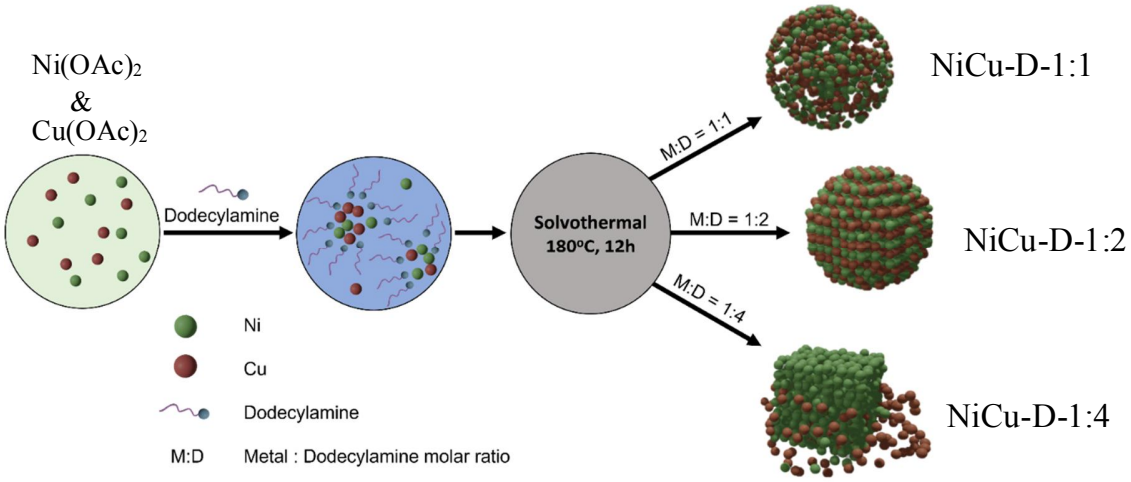

Figure 3.1. Schematic diagram of NiCu-D electrocatalysts preparation

Elemental mapping analysis (Figure 3.2(g) to (j)) showed that the sphere comprised evenly distributed Ni and Cu elements. Moreover, Ni also developed a cloud-like structure that befogged the sphere, creating a vast interaction area and faster mass transfer of reactive species from the electrolyte to the catalytic active sites. As the M:D increased to 1:4, the NiO was further reduced to form cubic Ni metal, which is proved by both FE-SEM micrographs and XRD patterns (Figure 3.3). The hierarchical structure has been broken due to the strong metal bonds that prioritize the growth of crystals, whose rigid crystalline barrier is not favorable for an efficient electrochemical reaction.

$$M^{2+} + 6CH_3(CH_2)_{11}NH_2 \rightarrow (CH_3(CH_2)_{11}NH_2)_6M^{2+} \quad (8)$$

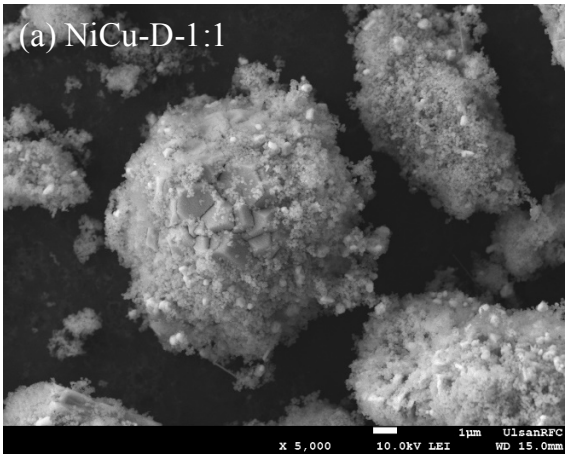
(a) NiCu-D-1:1
1μm UlsanRFC
X 5,000 10.0kV LEI WD 15.0mm


(b) NiCu-D-1:1
1μm UlsanRFC
X 10,000 10.0kV LEI WD 15.0mm

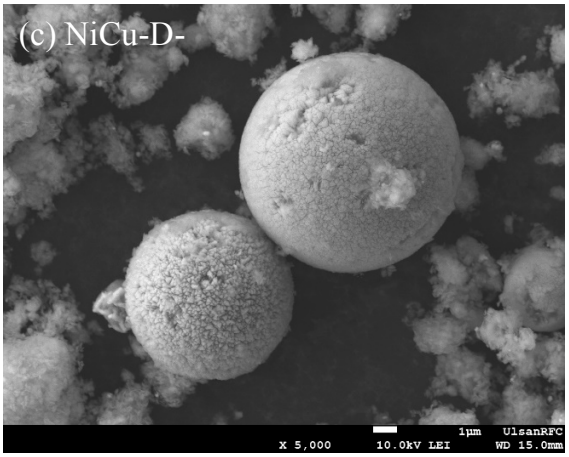
(c) NiCu-D-
1μm UlsanRFC
X 5,000 10.0kV LEI WD 15.0mm

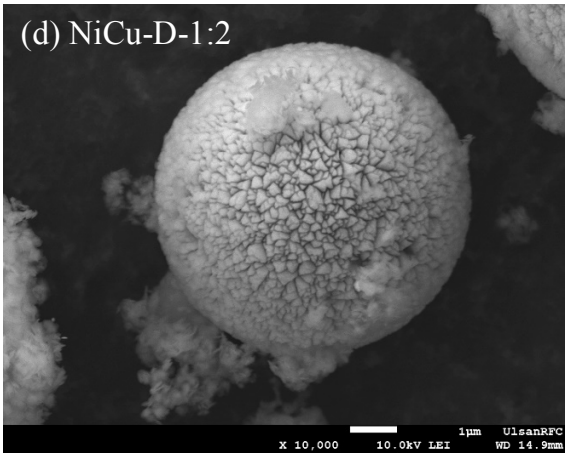
(d) NiCu-D-1:2
1μm UlsanRFC
X 10,000 10.0kV LEI WD 14.9mm


(e) NiCu-D-1:4
1μm UlsanRFC
X 5,000 10.0kV LEI WD 14.9mm

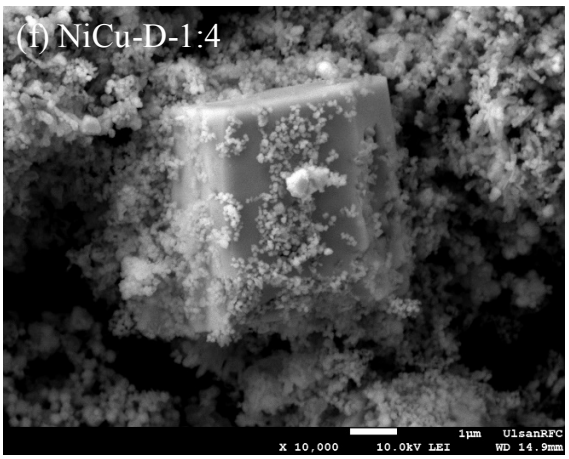
(f) NiCu-D-1:4
1μm UlsanRFC
X 10,000 10.0kV LEI WD 14.9mm

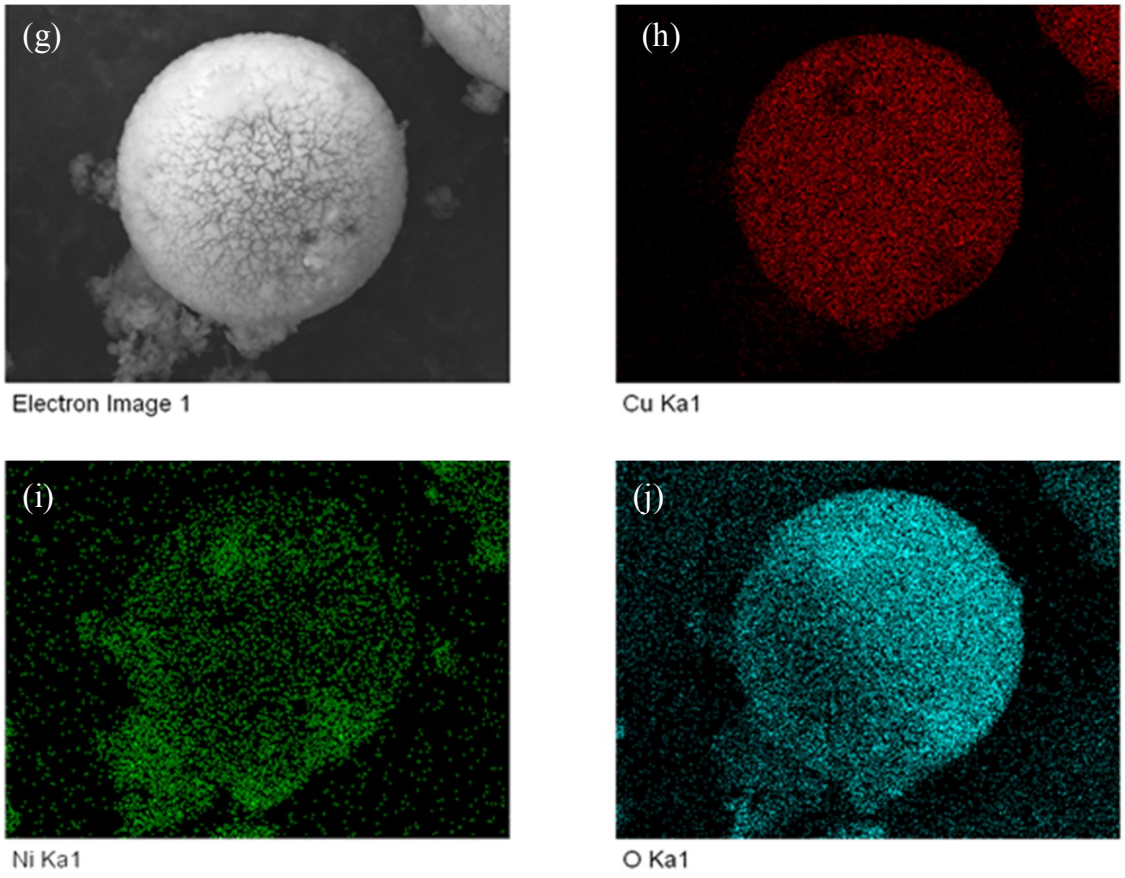

Figure 3.2. FE-SEM images of NiCu-based electrocatalysts with dodecylamine in different M:D, (a) and (b): NiCu-D-1:1, (c) and (d): NiCu-D-1:2, (e) and (f): NiCu-D-1:4, (g) to (j): elemental mapping of NiCu-D-1:2 catalyst

The phase composition of NiCu-D materials and Ni-D-1:2 was investigated using X-ray diffraction (XRD) analysis. As shown in (Figure 3.3), the M:D ratio has a great impact on the crystalline phases of the prepared materials. For both NiCu-D samples, the presence of Cu_2O and Cu was proved via the peaks at 2θ = 29.5, 36.5, 42.4, and 61.4° (Cu_2O – JCPDS 05-0667) and 2θ = 43.6, 50.8, 74.4° (Cu – JCPDS 04-0836) [50]–[52]. Neither peaks of CuO nor $Cu(OH)_2$ were found in the diffraction patterns. Besides, the decisive effect of dodecylamine on the properties of catalysts can be seen through the change in the phase of Ni concerning the M:D ratio. Polymorphous α-$Ni(OH)_2$ diffraction peaks at 2θ = 9.7, 33.5, and 59.8°, with β-$Ni(OH)_2$ at 19.9, 33.4, 38.6, 52.1, 59.8, and 63.4° could only be observed in NiCu-D-1:2 and Ni-D-1:2 [53]–[57]. While in NiCu-D-1:1 and NiCu-D-1:4, both peaks located at 37.2 and 62.7° can be assigned to NiO of (111) and (220) facets, respectively (JCPDS 73-1523) [58]–[60]. As mentioned above, the high amount of dodecylamine resulted in the reduction reaction to form cubic Ni metal, whose characteristic peaks appeared at 44.5 and 51.9° ((111) and (200) facets of JCPDS 04-850) [50], [61]. Although controlling catalytic crystalline phases is particularly important to design a high-performance material, our research group has not satisfyingly figured out the mechanism explaining the phase induction of dodecylamine. Therefore, this phenomenon would be discussed further in our next paper.

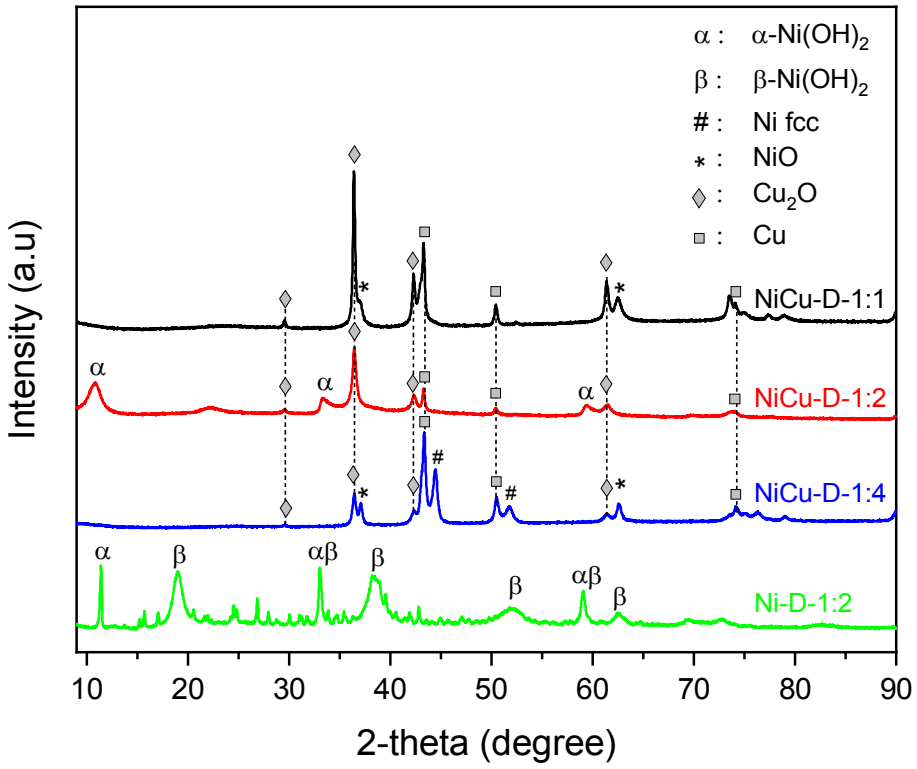

Figure 3.3. XRD patterns of NiCu-D and Ni-D-1:2 catalysts

To get a better understanding of the chemical states of the NiCu-D-1:2 sample, and explore the electronic changes during the AOR process, X-ray photoelectron spectroscopy (XPS) was conducted for NiCu-D-1:2/CP before and after AOR experiment. As shown in Figure 3.4, before AOR, two peaks of Ni^{2+} at 853.8 and 871.4 eV had higher intensity than the peaks of Ni^{3+} at 855.7 and 873.1 eV, indicating the presence of $Ni(OH)_2$ at the electrode surface [62]–[64] However, after AOR, Ni^{3+} peaks became prominent as a result of the formation of oxyhydroxide NiOOH, which was widely described as the active species for ammonia oxidation. Similarly, after AOR, two peaks corresponding to Cu(I) and Cu(0) at 933.6 and 932.3 eV were replaced by the peak of Cu(II) at 933.9 eV, implying the appearance of highly oxidative CuO [65]. In addition, the deconvolution of O1s spectra showed a major shift from O^{2-} peak at 529.7 eV to OH^- peak at 531.8 eV, indicating the adsorption of OH^- species in an alkaline solution. From this point of view, we can accomplish that throughout the AOR process, NiOOH and CuO formed on the electrode surface and served as the active sites for NH_3 oxidation [26], [66]–[70]. Meanwhile, OH^- can be adsorbed from the bulk solution and used as a proton carrier in the dehydrogenation process [71]. This information would be used to explain the mechanism of AOR, as demonstrated in Section 3.5 below.

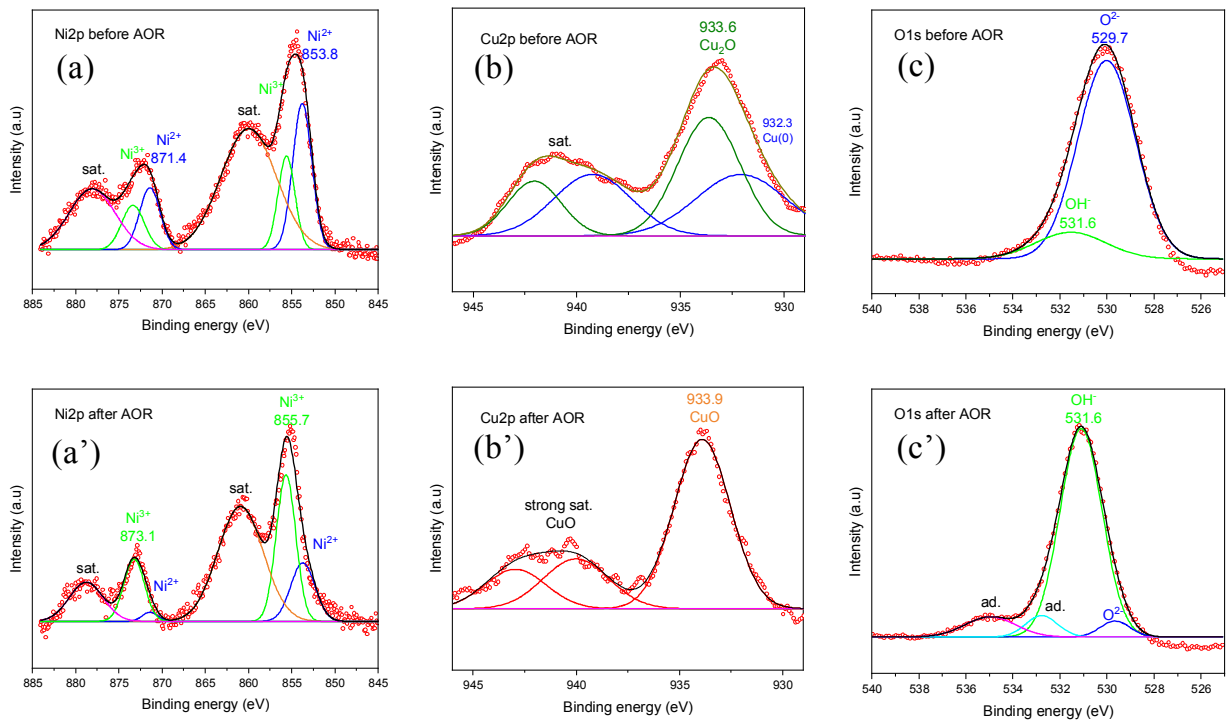

Figure 3.4. XPS spectra of NiCu-D-1:2/CP electrode before and after AOR experiments, (a) and (a') Ni2p before and after AOR, (b) and (b') Cu2p before and after AOR, (c) and (c') O1s before and after AOR

3.2. Electrochemical oxidation of ammonia

After drop-casting the materials onto the CP surface and employing activation, electrochemical experiments were conducted to evaluate the AOR activity of the electrodes. The synergistic effect of Ni and Cu towards NH_3 oxidation can be seen accordingly. As shown in Figure 3.5(a) and (b), after the introduction of NH_4Cl to the electrolyte solution, the current density of the Ni-D-1:2/CP electrode was almost unchanged. On the contrary, we found a significant increase in the response current of NiCu-D/CP electrodes in the presence of NH_3, proving their high AOR reactivity. NiCu-D-1:2/CP showed the highest reactivity of 44.9 mA/cm^2 at 0.6 V, while either samples with lower or higher dodecylamine dosage would limit the resulting performance. In the case of NiCu-D-1:1/CP electrocatalyst, the concentration of surfactant is insufficient to promote structural arrangement, hence an optimal surface exposure was not obtained. On the other hand, the over-addition of dodecylamine in NiCu-D-1:4/CP led to the reduction of oxide to metallic Ni and Cu, whose rigid crystalline structures prevents high activity [26], [72] It is worth noting that the intensity of the CV peak of Ni-D-1:2/CP should not be used for comparison, since it is solely related to the oxidation of Ni^{2+} to Ni^{3+} and not AOR.

The metal/dodecylamine molar ratio affected not only the activity but also the thermodynamics as well as the kinetics of AOR. As shown in LSV curves in Figure 3.5(c), NiCu-D-1:2/CP represented the lowest onset potential of 0.46 V vs Hg/HgO, compared to around 0.52 V of NiCu-D-1:1/CP and NiCu-D-1:4/CP. Since the onset potential represents the

feasibility of a reaction, its reduction indicates a more favorable thermodynamic. Also, the corresponding Tafel plots exhibited that NiCu-D-1:2/CP has a Tafel slope of 28.9 mV/dec, which is much smaller than that of NiCu-D-1:1/CP (102.0 mV/dec) and NiCu-D-1:4/CP (87.8 mV/dec). As the Tafel slope represents the quantity of overpotential required to the current a factor of ten under the same conditions, a low value for NiCu-D-1:2/CP implies it possesses quick catalytic kinetics. Chronoamperometry test (CA – Figure 3.5(e)) was applied to assess the catalytic activity over a longer period. The catalytic activity was ordered as NiCu-D-1:2/CP > NiCu-D-1:1/CP > NiCu-D-1:4/CP >> Ni-D-1:2/CP, which was consistent with the CV experiment. As the reaction time increased, the current density slightly decreased, which resulted from the reduction of NH_3 concentration given over time rather than the electrode stability. To validate our assumption, we conducted a separate experiment, as shown in Figure 3.6. The result demonstrated that NiCu-D-1:2/CP after 9 hours of electrolysis returned to the same initial anodic current when the old electrolyte was replaced by the new one, confirming the reliable stability of the catalyst.

EIS is a powerful technique for diagnosing the intrinsic characteristics of the catalysts and reaction processes. The Nyquist plots of the electrodes were well-fitted by the well-known Randle's circuit as shown in the inset in Figure 3.5(f) and Table 3.2. The plots consisted of semicircles with different diameters and a linear line inclined at an angle of 45^o. The diameter values of semicircles revealed the charge transfer resistance (R_{ct}, inset circuit) of the reaction. Therefore, a smaller semicircle of NiCu-D-1:2/CP ulteriorly demonstrates the faster charge

transfer at the electrode/electrolyte interface compared to other electrodes, approving its enhanced AOR performance. Furthermore, the tilted linear line is the characteristic feature of a Warburg element, representing the impedance of diffusion of reactive species from the bulk solution to the electrode-electrolyte interface. The presence of the line indicates that the reactivity was controlled by not only the intrinsic properties of the catalysts but also the mass transfer of NH_3 in the solution. Therefore, the enhancement in the extrinsic variable (temperature, NH_3 concentration, convection, etc.) could strongly affect the rate of the process.

Finally, we compare the electrochemically active surface areas (ECSA) of the catalysts based on their linear correlation to the double-layer capacitance (C_{dl}) [73]. C_{dl} values of NiCu-D/CP and Ni-D-1:2/CP electrodes were calculated via CV experiment with different scan rates in the non-Faradaic region. As shown in Table 3.2 and Figure 3.7, the C_{dl} values increased with the increase of dodecylamine content, proving the surface activity of dodecylamine. As a consequence, NiCu-D-1:4/CP provided the largest active area even though it is not the most efficient catalyst. It exhibited that the electroactive species which are participating in the reaction also have an important role in the electrochemical activity; as the XRD result confirmed Ni exists in the form of metallic Ni in NiCu-D-1:4, whilst it appears in the form of Ni(OH)2 in Ni-D-1:2.

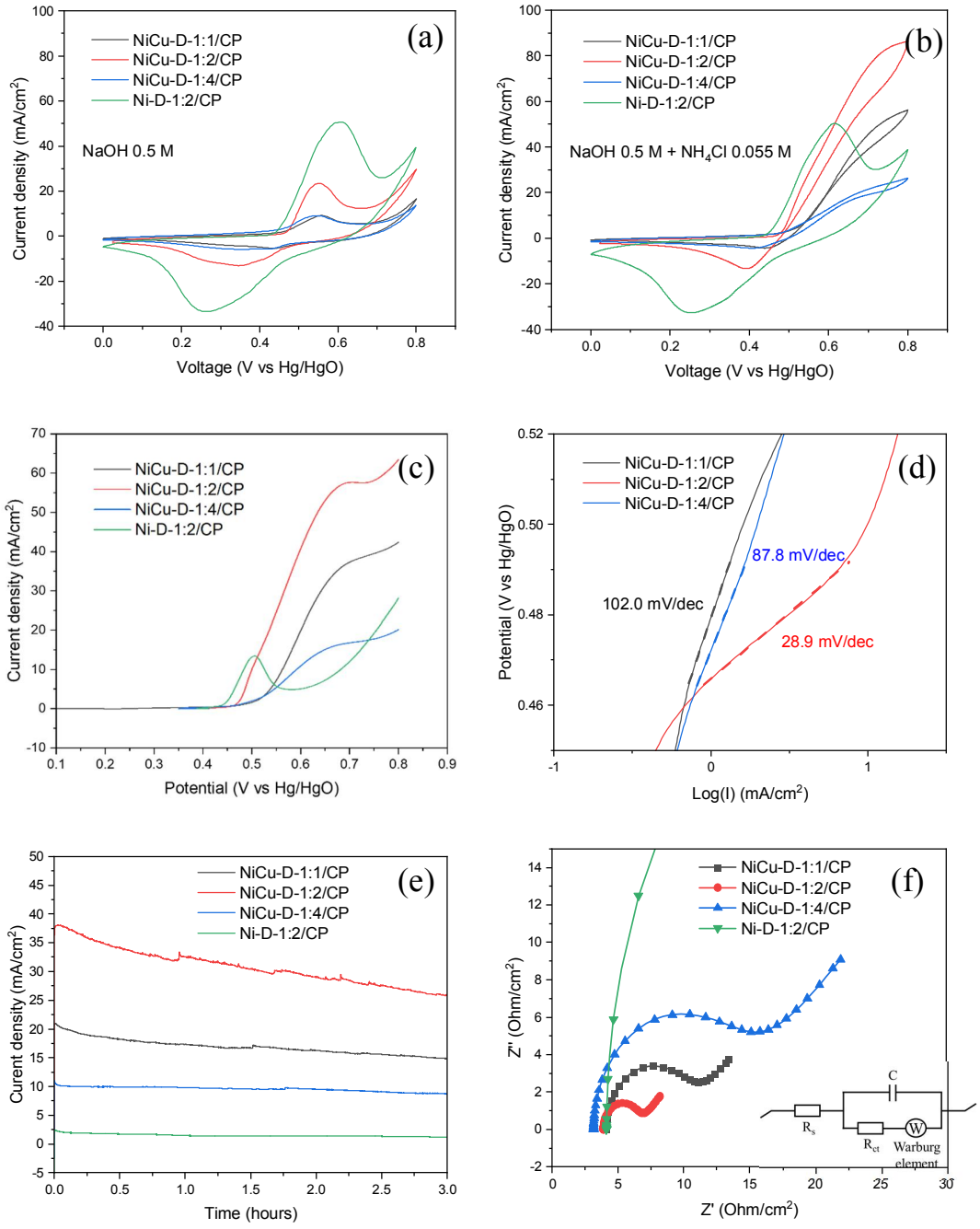

Figure 3.5. (a) and (b) Cyclic voltammograms (CV) of dodecylamine-based electrodes in NaOH 0.5M without and with NH_4Cl 0.055M, (c) LSV curves of dodecylamine-based electrodes, (d) Tafel plots of NiCu-D/CP electrodes, (e) chronoamperometry curves and (f) Nyquist plot of dodecylamine-based electrodes

Table 3.1. AOR activities of different electrocatalysts

Catalysts	Test conditions	E (V)	Performance	Ref.
NiCu-D-1:2	55 mM NH_4Cl + 0.5 M NaOH, 25 mV/s	0.6 V vs Hg/HgO	44.9 $mAcm^{-2}$	This work
$Ni_{0.8}Cu_{0.2}LHS$	55 mM NH_4Cl + 0.5 M NaOH, 25 mV/s	0.55 V vs Ag/AgCl	36 $mAcm^{-2}$	[66]
$NiCu/MnO_2$	55 mM NH_4Cl + 0.5 M NaOH	0.7 V vs Hg/HgO	25 $mAcm^{-2}$	[74]
NiCu/CP	55 mM NH_4Cl + 0.5 M NaOH, 20 mV/s	0.6 V vs Ag/AgCl	30 $mAcm^{-2}$	[50]
Ni_1Cu_3-S-T/CP	0.2 M NH_4Cl + 1 M NaOH, 20 mV/s	1.69 V vs RHE	110 $mAcm^{-2}$	[26]
Ni_2P/NF	0.36 M NH_3 + 0.1 M KOH, 5 mV/s	1.65 V vs RHE	10 $mAcm^{-2}$	[62]
$Ni(OH)_2$-Cu_2O@CuO	1 M KOH + 1 M NH_3, 20 mV/s	0.6 V vs Hg/HgO	60 $mAcm^{-2}$	[75]
$Ni_{50}Cu_{50}/CNT$	0.5 M NH_3 + 1 M KOH, 20 mV/s	0.6 V vs Hg/HgO	85 $mAcm^{-2}$	[76]
$PtIrNi_1/SiO_2$-CNT-COOH	0.1 M NH_3 + 1 M KOH, 5 mV/s	0.7 V vs RHE	120 (A/g)	[77]

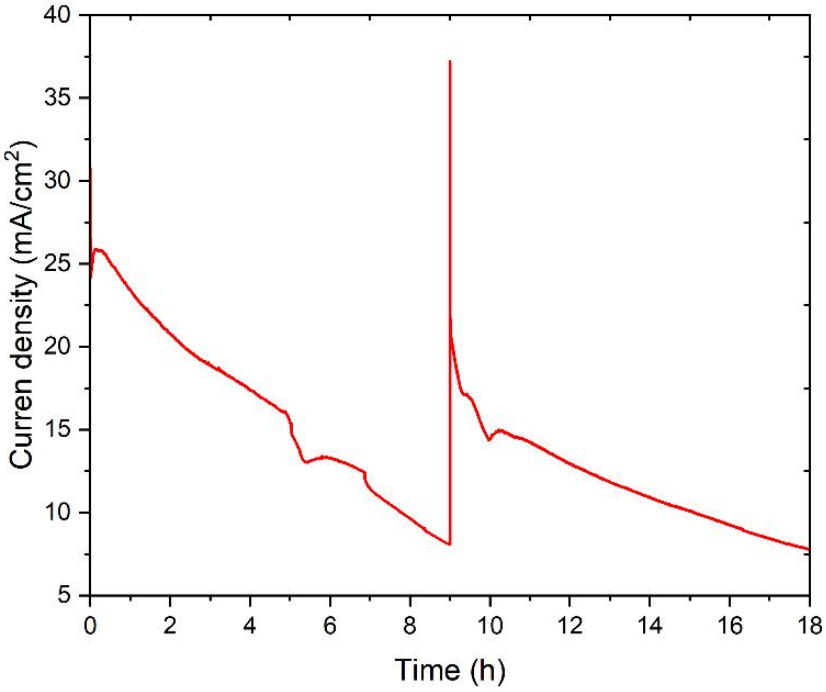

Figure 3.6. Stability test of NiCu-D at 0.6 V vs Hg/HgO.

Table 3.2. Parameters of EIS measurements of NiCu-D-1:1/CP, NiCu-D-1:2/CP, NiCu-D-1:4/CP, and Ni-D-1:2/CP

NiCu-D-1:1/CP	NiCu-D-1:2/CP	NiCu-D-1:4/CP	Ni-D-1:2/CP
$R_1+C_1/(R_2+W_2)$	$R_1+C_1/(R_2+W_2)$	$R_1+C_1/(R_2+W_2)$	$R_1+C_1/(R_2+W_2)$
R_1 = 4.107 Ω	R_1 = 3.905 Ω	R_1 = 3.151 Ω	R_1 = 4.133 Ω
C_1 = 6.17 mF	C_1 = 5.68 mF	C_1 = 2.81 mF	C_1 = 78.08 mF
R_2 = 6.13 Ω	R_2 = 2.635 Ω	R_2 = 10.8 Ω	R_2 = 65.6 Ω
s_1 = 2.74 $\Omega s^{-1/2}$	s_1 = 1.36 $\Omega s^{-1/2}$	s_1 = 6.80 $\Omega.s^{-1/2}$	s_1 = 1.01 $\Omega.s^{-1/2}$

Table 3.3. Double layer capacitance of the NiCu-D/CP and Ni-D-1:2/CP electrodes

Electrodes	Double layer capacitance (C_{dl}) (mF/cm^2)
NiCu-D-1:1/CP	10.64
NiCu-D-1:2/CP	12.54
NiCu-D-1:4/CP	14.22
Ni-D-1:2/CP	11.5

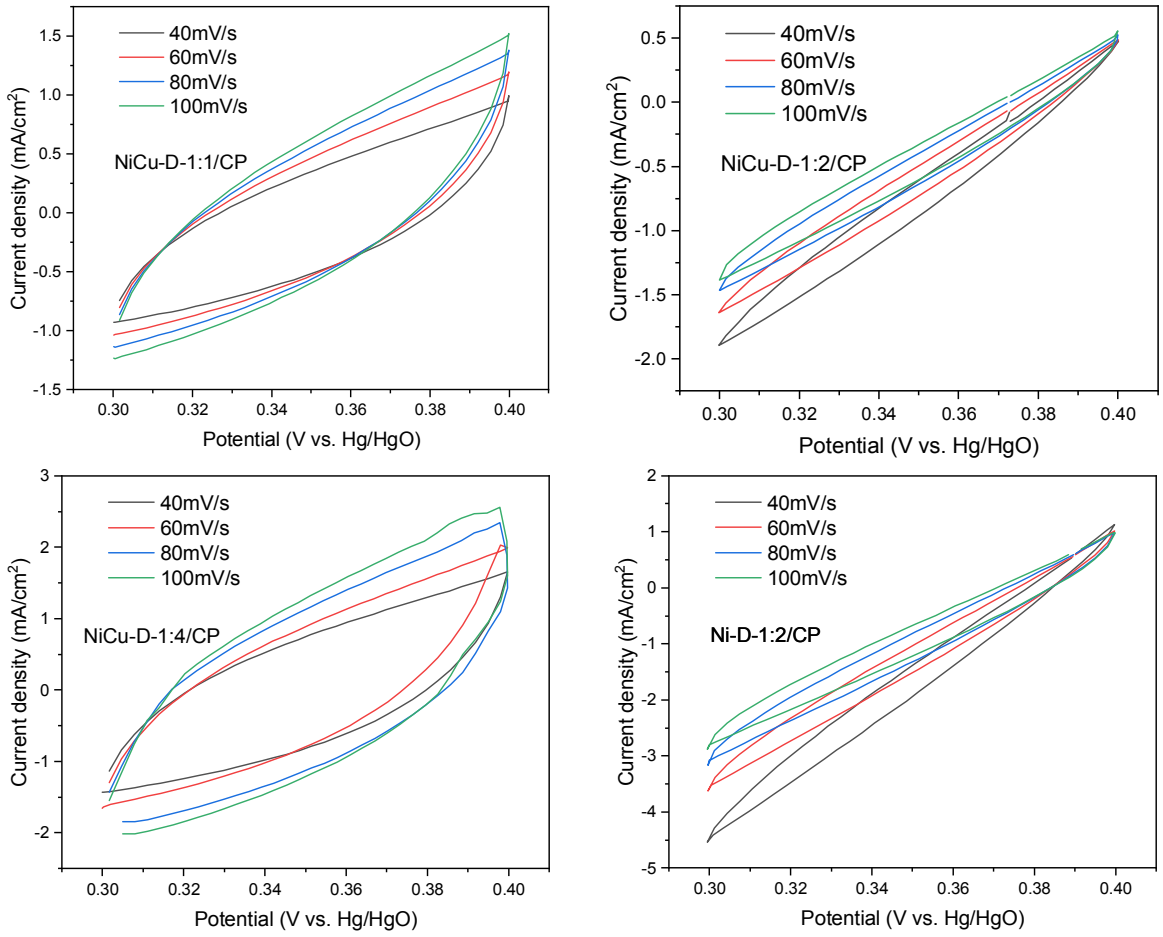

Figure 3.7. CV measurements with different scan rates of dodecylamine-based electrodes

3.3. Effects of different precipitation agents on AOR activity of NiCu-electrocatalysts

In material science, precipitation agents have a decisive role in the structure, property, and catalytic activity of the synthesized catalysts. Herein, we investigate the effects of several common precipitation agents including urea, NaOH, NH_3, and TEA on the AOR activity of NiCu-based electrocatalysts. Although all the catalysts originated from the same Ni and Cu salts and solvent, the change in precipitation agent led to the formation of different morphologies (shown in SEM images, Figure 3.8) and ECSA values (Table 3.4). NiCu-D-1:2, with its unique morphology, showed the highest C_{dl} value compared to other catalysts.

Table 3.4. Double layer capacitance of the NiCu electrodes made from different precipitation agents

Electrodes	Double layer capacitance (C_{dl}) (mF/cm^2)
NiCu-D-1:2/CP	12.54
NiCu-Urea/CP	8.34
NiCu-NaOH/CP	6.80
NiCu-NH_3/CP	6.66
NiCu-TEA/CP	4.86

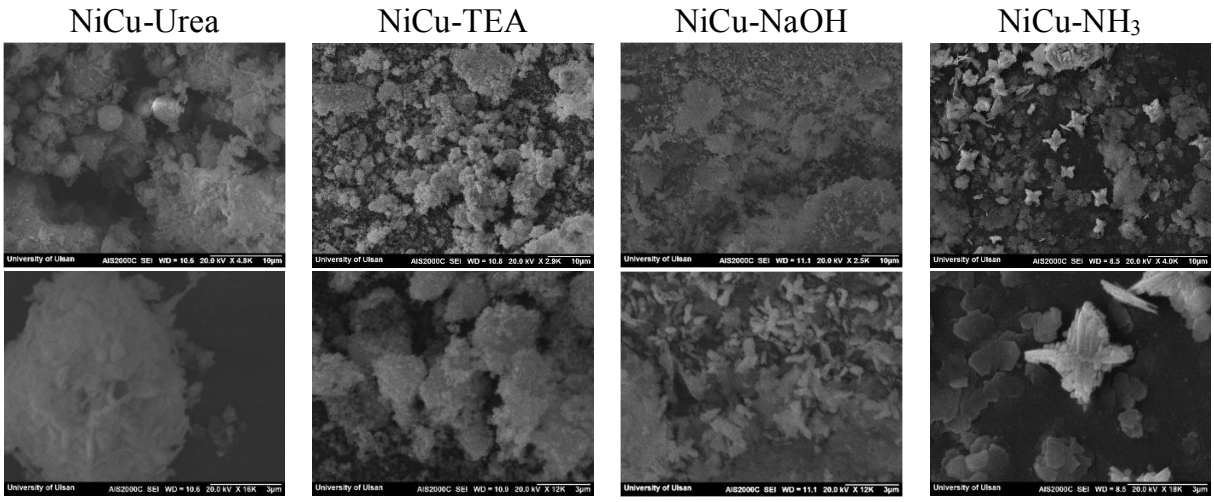

Figure 3.8. SEM images of NiCu-Urea, NiCu-TEA, NiCu-NaOH, and NiCu-NH3

The activities towards AOR were measured via electrochemical experiments, as shown in Figure 3.9 and Figure 3.10. The corresponding current density from CV tests varied significantly among the surveyed precipitation agents with the order of dodecylamine> urea > TEA > NaOH > NH_3. Based on the results, the precipitation agent plays a key role in determining two important parameters for electrochemical reactivity comprising active species and also the corresponding morphology which directly controls electrochemical active surface area.

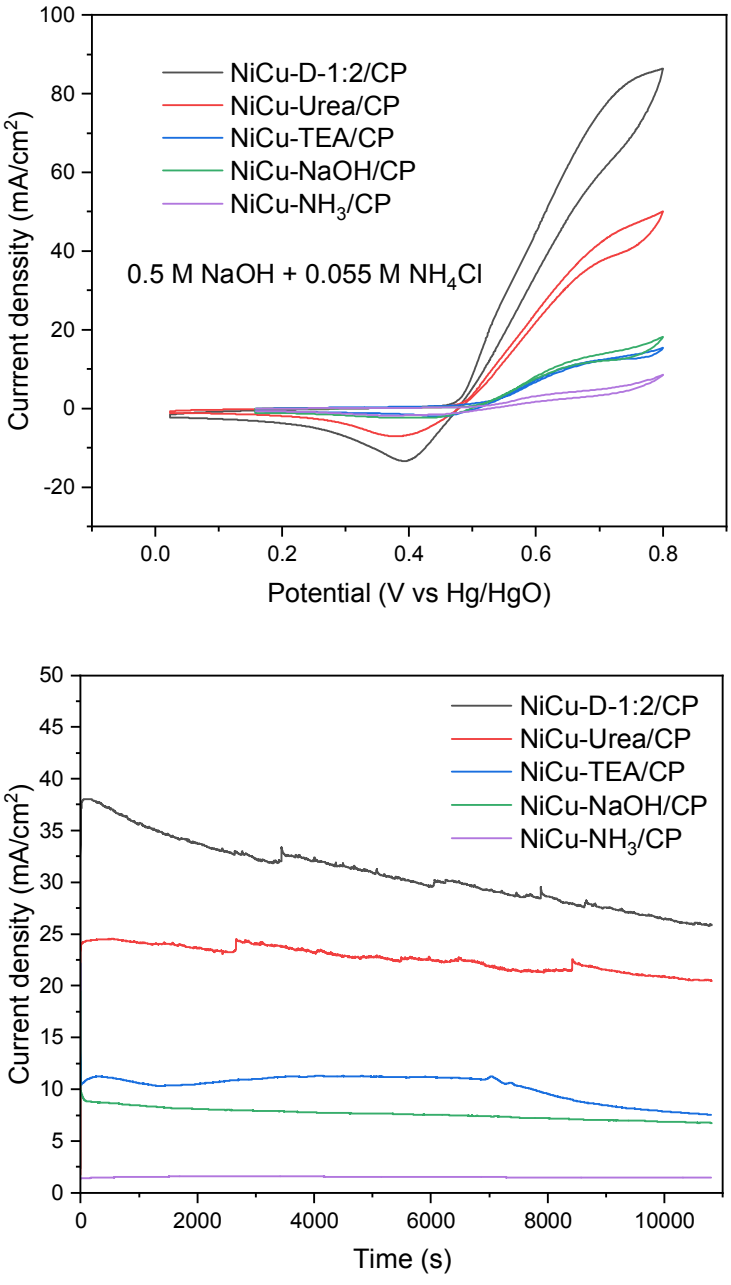

Figure 3.9. Cyclic voltammetry of prepared catalysts in NaOH with and without NH_3, scan rate: 25mV/s

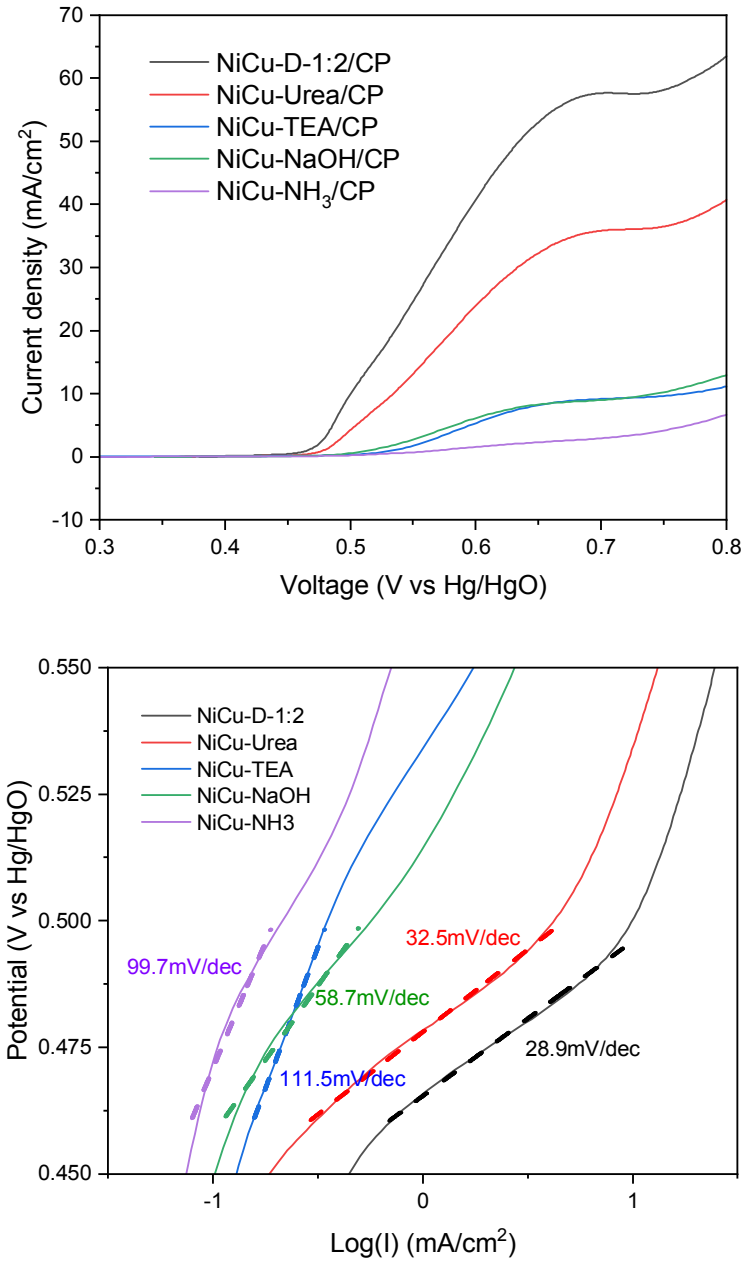

Figure 3.10. LSV and Tafel slopes of synthesized electrocatalysts

3.4. Ammonia removal test and selectivity of the products

We measured the NH_3 removal performance of NiCu-D-1:2/CP, our most efficient electrode, NiCu-Urea/CP, and the bare Ni-D-1:2 to study the ammonia electrooxidation reaction. NiCu-Urea/CP has been chosen because it was made from urea, a frequently used precipitation agent for nickel-based hydroxide electrocatalysts. For a particular test, a catalyst-coated CP electrode with an area of 0.5 cm^2 was immersed into a 30 mL electrolyte containing 0.5 M NaOH and 0.05 M NH_4Cl. The experiment was conducted under a constant voltage of 0.6 V (vs Hg/HgO) for 9 hours straight. We calculated the energy efficiency by assuming all charge transfer was utilized for ammonia oxidation to N_2 without forming any by-products or water oxidation interference. Hence, the energy efficiency could be calculated according to equation (9):

$$\varepsilon_f = \frac{Fn_e(C_0 - C_i)\,V}{Q} \tag{9}$$

where F is the Faraday constant of 96485 sA/mol, n_e is the number of electrons transferred in half-reaction, for ammonia oxidation to N_2, n_e is the number of electrons transferred, C_0 and C_i are molar concentrations of ammonia at t = 0 and at each time interval, respectively (M), V

is the volume of the electrolyte, here we use V = 0.03 L, and Q is the number of electrons supplied from the potentiostat (Coulomb).As shown in Figure 3.11(a), the concentration of ammonia reduced consistently with working time and NiCu-D-1:2/CP showed much better activity in NH_3 removal as compared to NiCu-Urea/CP and Ni-D-1:2/CP. The energy efficiency calculation showed that NiCu-D-1:2/CP utilized around 60 % of supplied energy for NH_3 oxidation, while it was just 48 % for NiCu-Urea/CP. The difference might come from either the intrinsic effectiveness of the materials or the dissimilarity in the distribution of products. In other words, the calculation with the assumption of all reacted NH_3 turned to N_2 is not practically correct because some by-products such as NO_2^- and NO_3^- were also formed along the electrolysis.

As AOR proceeded, the anode could either release N_2 gas or toxic NO_x ions into the solution. Therefore, the quantitative analysis of the products plays a pivotal role in determining the environmental impact of the process, as well as a deep study of the mechanism behind it. Herein, we utilized an *in-operando* GC-TCD system to quantify the products of the ammonia electrooxidation reaction with respect to time. A detailed description of the experiment was demonstrated in the Experimental section. Faradaic efficiencies (ε %) were demonstrated for N_2, O_2 gases and NO_x via equations (10) to (12) below:

$$\varepsilon_{N_2\,path} = \frac{[N_2] \times 6 \times \upsilon \times \Delta t \times F}{Q} \times 100\ \% \tag{10}$$

$$\varepsilon_{O_2\,path} = \frac{[O_2] \times 4 \times \upsilon \times \Delta t \times F}{Q} \times 100\ \% \tag{11}$$

$$\varepsilon_{NO_x\,path} = 100\ \% - \varepsilon_{N_2\,path} - \varepsilon_{O_2\,path} \tag{12}$$

where Q is the total charge supplied (coulomb); υ is the flow rate of Ar gas; and F is the Faraday constant (96485 C/mol). The obtained Faradaic efficiencies for NiCu-D-1:2/CP, NiCu-Urea/CP, and Ni-D-1:2/CP electrodes were illustrated in Figure 3.11(b) to (d). In all electrodes, the O_2 percentages were minor due to the insufficient applied potential for oxygen evolution reaction. However, the Faradaic efficiency of N_2 and NO_x markedly differed in the three surveyed electrodes. Interestingly, the percentages of N_2 formation in the Cu-containing electrodes (NiCu-D-1:2/CP and NiCu-Urea/CP) were much higher than that of the Cu-free one (Ni-D-1:2/CP). In addition, we also found that NiCu-D-1:2/CP had a higher N_2 selectivity (78 %) as compared to that of NiCu-Urea/CP (46 %). As far as our concern, the selectivity of AOR reaction is still receiving mixed results and opinions. Therefore, in the next part, we aim to clarify the mechanism behind the product selectivity of ammonia electrolysis, and how NiCu could prioritize N_2 formation as well as promote an effective AOR activity.

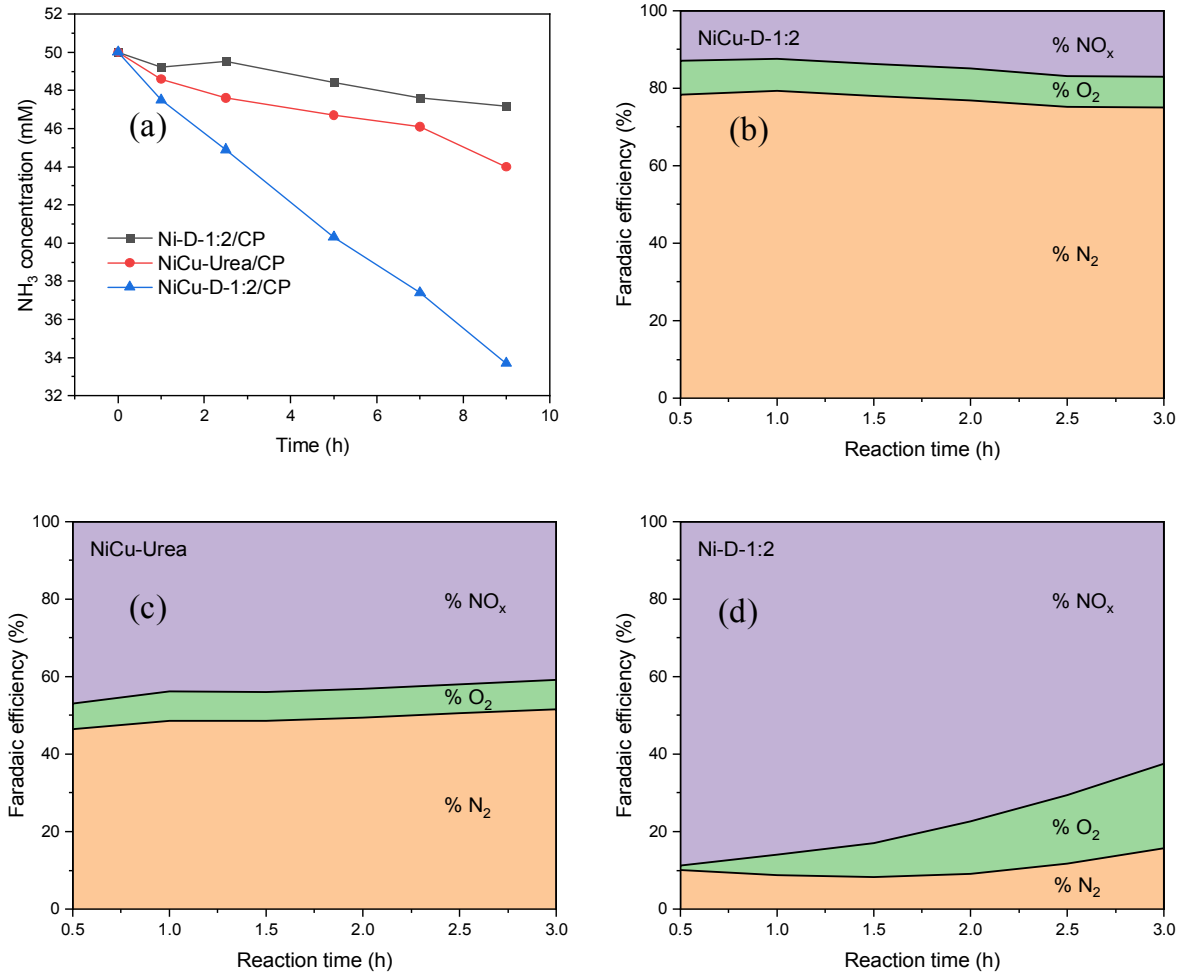

Figure 3.11. (a) NH_3 removal and (b), (c), (d) Faradaic efficiency of NiCu-D-1:2/CP, NiCu-Urea/CP, and Ni-D-1:2/CP at 0.6V vs Hg/HgO, respectively

3.5. Unique synergistic effect of Ni and Cu in AOR

So far, there are two AOR reaction mechanisms that have been recognized: G-M and O-S (Mechanism 1 and 2). Numerous investigations have shown that the G-M route has a lower onset potential and is easier to take place at low voltages than O-S pathway. Moreover, the dimerization step in the G-M mechanism may also intrinsically favor N_2 selectivity over NO_x as it competes with creation of N* species, which are the precursors of NO_x. To have an explanation of those phenomena, we utilized the data on free energy from research by Herron et al. to elucidate the constraints of Ni and explain how Cu can improve the overall AOR process [14].

The free-energy data of adsorbed species on catalyst surfaces are provided in Table 3.5, Table S1-S2, and the minimum energy pathway of AOR on Ni(111) and Ni(111)-Cu(111) facets were respectively illustrated in **오류! 참조 원본을 찾을 수 없습니다.**. For pure Ni (**오류! 참조 원본을 찾을 수 없습니다.**(a)), the minimum energy pathway follows the eventual dehydrogenation of NH_3-derived species to form NH_2* and NH*. Then two different pathways could take place: for the G-M pathway, NH_2* and NH* dimerize to form H_2N-NH*, which is furthered deprotonated to the final N_2; while in O-S pathway, deprotonation continues to occur on NH* to form N*, which can either dimerize to form N_2 or eventually be oxidized to NO_x species. Thermodynamically, the potential-determining step of G-M pathway is the deprotonation of H_2N-NH* to HN-NH* with ΔG = 0.33 eV, much lower than that of 0.56 eV

of O-S pathway, which belongs to the deprotonation of NH* to N*. Therefore, the G-M route requires less energy and lower onset potential than O-S mechanism. Unfortunately, studies have shown that AOR on Ni materials is more likely to follow the O-S mechanism, resulting in limited current response and low N_2 selectiveness of Ni-based catalysts. We inferred that because the sluggish dimerization step $NH_2^* + NH^* \rightarrow H_2N\text{-}NH^*$ prevent the occurrence of G-M pathway, as its energy barrier of 1.22 eV is too large for any practical reaction to take place. The introduction of Cu to Ni could effectively solve this problem. As shown in **오류! 참조 원본을 찾을 수 없습니다.**(b), the NH_2^* species generated on Ni surface could be transferred to Cu, whose lower energy barrier of dimerization step, to conduct the dimerization reaction. In other words, Cu facilitates the G-M route as it cuts down the energy barrier of dimerization, leading to a more feasible reaction and lower onset potential. Furthermore, the addition of Cu to Ni can enhance the selectiveness of the material. As G-M pathway is prioritized, the formation of N* species, which is the main source of precursor of NO_x, was constrained. Consequently, the selectivity toward N_2 of NiCu electrodes will be enhanced compared with the sole Ni.

Table 3.5. Gibbs Free Energy of Adsorbed Intermediates at 0 V Relative to $N_2(g)$, $H_2O(g)$, and OH^- (Reused with ACS permission)

	N	NH	NH_2	NNH	HNNH	NNH_2	$HNNH_2$	H_2NNH_2
Ni	0.23	-0.33	-0.21	0.97	1.00	0.58	0.68	0.97
Cu	1.94	0.71	0.27	2.08	1.87	1.78	1.40	1.21
Pt	0.79	0.27	0.10	1.16	1.16	1.08	1.03	0.75

All values are in electronvolts. The Gibbs free energy of $NH_{3(g)}$ is calculated to be -0.36 eV.

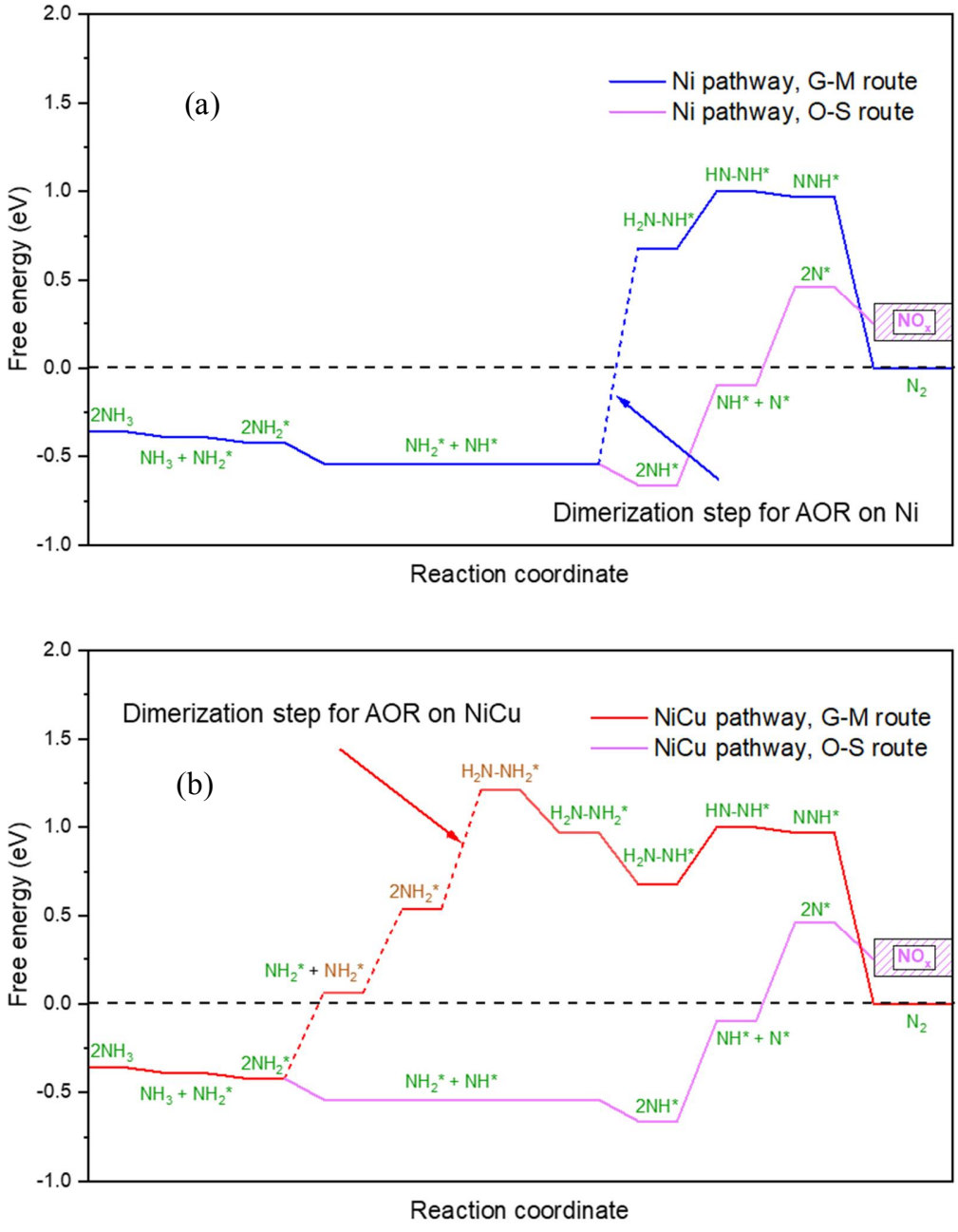

Figure 3.12. Free-energy diagram of the minimum-energy pathway for ammonia electrooxidation on (a) Ni (111) and (b) Ni(111) with Cu(111) at 0 V vs. RHE. Zero energy corresponds to N2(g). The green and brown words represent the species adsorbed on nickel and copper

Aside from the nature of the material, the coverage degree, e.g., concentration, of NH_x* and NH_y* has a great impact on the dimerization step. For the formation of one dimerized N_2H_{x+y} species, two adjacent arbitrary NH_x* and NH_y* are required rather than a single one. Meanwhile, the probability of the two species being adjacent is proportional to the square of the electrochemical active surface area, $ECSA^2$. As a result, the increase in ECSA significantly enhances the rate of the dimerization step and turns the reaction towards the G-M pathway. Combine with the data we obtained from XPS analyses, we proposed a unique mechanism for AOR reaction on NiCu-based materials, as shown in Figure 3.13 and Equation (13) – (23). During the reaction, NiOOH, and CuO was formed and acted as the active species for AOR. Meanwhile, the minimum-energy reaction route showed that Ni is responsible for dehydrogenation steps, and Cu is the active site for dimerization. The synergy of the two metals promotes the synthesis of robust electrocatalysts with a high N_2 selectivity.

$$Ni^{2+}(OH)_2 + OH^- \rightarrow Ni^{3+}OOH + H_2O + e^- \quad (13)$$

$$Ni^{3+}OOH + NH_3 \rightarrow Ni^{3+}OOH - NH_{3(ads)} \quad (14)$$

$$Ni^{3+}OOH - NH_{3(ads)} \rightarrow Ni^{2+}O - NH_2 + H_2O \quad (15)$$

$$Ni^{2+}O - NH_2 + H_2O + OH^- \rightarrow Ni^{3+}OOH - NH_2 + e^- \quad (16)$$

$$Ni^{3+}OOH - NH_2 \rightarrow Ni^{2+}O - NH + H_2O \quad (17)$$

$$Ni^{2+}O - NH_x + Cu^{2+} \rightarrow Ni^{2+}O + Cu^{2+} - NH_x \quad (18)$$

$$Cu^{2+} - NH_x + Cu^{2+} - NH_y \rightarrow Cu^{2} - N_2H_{x+y} \quad (19)$$

$$Cu^{2+} - N_2H_{x+y} + Ni^{2+}O \rightarrow Ni^{2+}O - N_2H_{x+y} + Cu^{2+} \quad (20)$$

$$Ni^{2+}O - N_2H_{x+} + H_2O + OH^- \rightarrow Ni^{3+}OOH - N_2H_{x+y} \quad (21)$$

$$Ni^{3+}OOH - N_2H_{x+y} \rightarrow Ni^{2+}O - N_{2(ads)} + H_2O \quad (22)$$

$$Ni^{2+}O - N_{2(ads)} \rightarrow Ni^{2+}O + N_2 \quad (23)$$

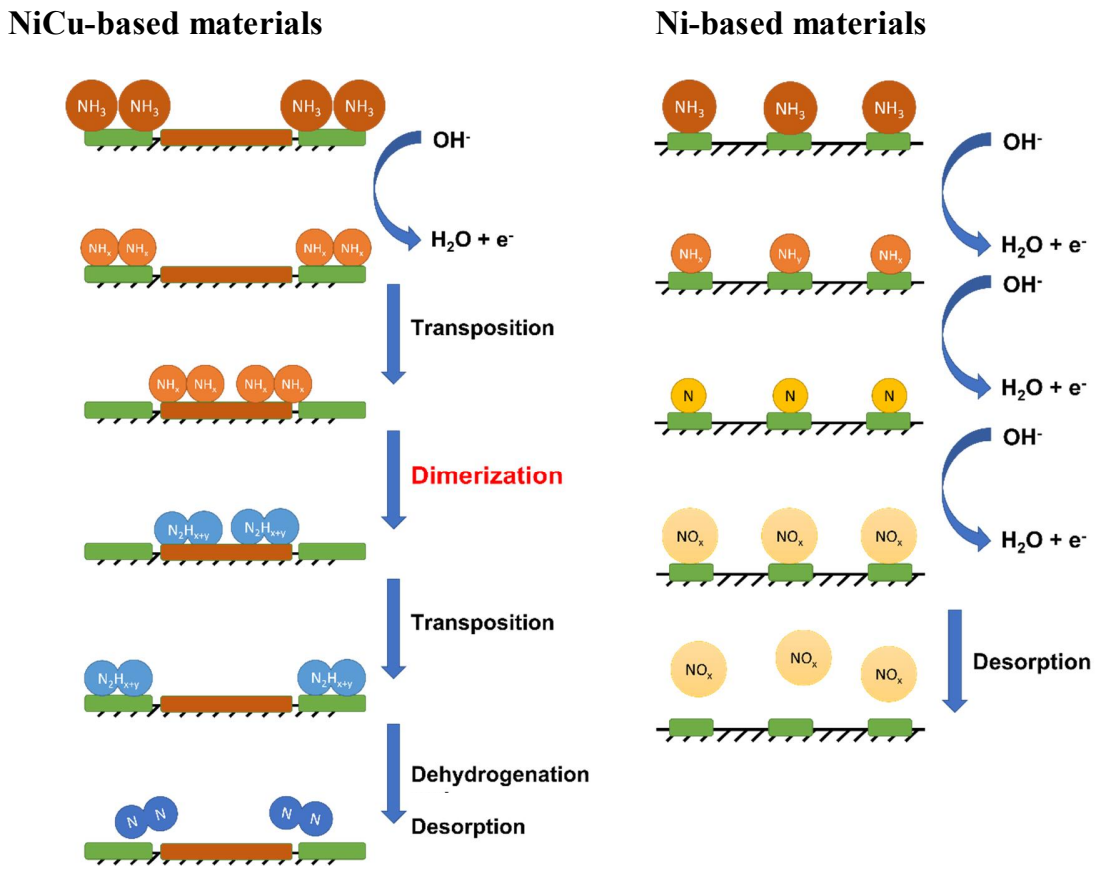

Figure 3.13. Plausible AOR mechanism towards N_2 and NO_x formation

CHAPTER 4: CONCLUSION

In summary, a new type of NiCu-based electrocatalyst with well controlled-morphology has been successfully constructed via a facile one-step solvothermal method for AOR applications. By using dodecylamine as the precipitation agent, the resulted materials showed ordered morphologies, which could be engineeringly controlled by changing the metal salt to dodecylamine ratio. Compared to several well-known precipitation agents, the use of dodecylamine promotes drastic enlargement in the active surface area of the synthesized samples. The optimal ratio of 1:2 promotes the synthesis of a prominent NiCu-D-1:2 catalyst with a unique spherical shape that enables active site exposure and effortless diffusion. Consequently, NiCu-D-1:2/CP electrode induced enhanced AOR performance with a current density of 44.9 mA/cm^2 in the CV experiment at 0.6 V vs Hg/HgO. Besides, an *in-operando* GC system revealed a high N_2 selectivity of NiCu-D-1:2/CP of 79 %. In order to explain the results, the free energy data were used to uncover a new mechanism pathway of NiCu-catalysts that could surpass the intrinsic disadvantages of each bare metal by utilizing individual's strength. As a result, Ni and Cu can perform different functions in AOR process, therefore following a new reaction pathway whose conversion rate and N_2 selectivity could be significantly enhanced. This paper not only introduces a facile synthesis of efficient materials but also provides valuable knowledge of AOR process, paving the way for the development of robust and highly selective electrocatalysts.

REFERENCES

[1] N. Hanada, S. Hino, T. Ichikawa, H. Suzuki, K. Takai, and Y. Kojima, "Hydrogen generation by electrolysis of liquid ammonia," *Chemical Communications*, vol. 46, no. 41, pp. 7775–7777, Nov. 2010, doi: 10.1039/c0cc01982h.

[2] H. Gerischer and A. Mauerer, "Untersuchungen Zur anodischen Oxidation von Ammoniak an Platin-Elektroden," *J Electroanal Chem Interfacial Electrochem*, vol. 25, no. 3, pp. 421–433, May 1970, doi: 10.1016/S0022-0728(70)80103-6.

[3] B. Bonnet-Cantalloube, M. Espitalier-Noël, P. Ferrari De Carvalho, J. Fonseca, and G. Pawelec, "Photo Cover © Justin Jin for Hydrogen Europe," 2023.

[4] U. National Minerals Information Center, "mcs2020.pdf - Mineral Commodity Summaries 2020."

[5] N. M. Adli, H. Zhang, S. Mukherjee, and G. Wu, "Review—Ammonia Oxidation Electrocatalysis for Hydrogen Generation and Fuel Cells," *J Electrochem Soc*, vol. 165, no. 15, pp. J3130–J3147, 2018, doi: 10.1149/2.0191815jes.

[6] I. Lucentini, X. Garcia, X. Vendrell, and J. Llorca, "Review of the Decomposition of Ammonia to Generate Hydrogen," *Ind Eng Chem Res*, vol. 60, no. 51, pp. 18560–18611, Dec. 2021, doi: 10.1021/acs.iecr.1c00843.

[7] T. A. Le, Q. C. Do, Y. Kim, T. W. Kim, and H. J. Chae, "A review on the recent developments of ruthenium and nickel catalysts for COx-free H2 generation by ammonia decomposition," *Korean Journal of Chemical Engineering*, vol. 38, no. 6. Springer, pp. 1087–1103, Jun. 01, 2021. doi: 10.1007/s11814-021-0767-7.

[8] C. Wu, S. Zheng, Z. Wang, R. Chen, X. Hu, and J. Chen, "Discussion on ammonia as one of the energy storage media of solar energy in China," *Energy Strategy Reviews*, vol. 38, p. 100697, Nov. 2021, doi: 10.1016/J.ESR.2021.100697.

[9] S. Padinjarekutt *et al.*, “Na+-gated nanochannel membrane for highly selective ammonia (NH3) separation in the Haber-Bosch process,” *Chemical Engineering Journal*, vol. 454, p. 139998, Feb. 2023, doi: 10.1016/j.cej.2022.139998.

[10] A. N. Petukhov *et al.*, “A highly-efficient hybrid technique – Membrane-assisted gas absorption for ammonia recovery after the Haber-Bosch process,” *Chemical Engineering Journal*, vol. 421, Oct. 2021, doi: 10.1016/j.cej.2020.127726.

[11] S. Khan, S. S. Shah, M. A. R. Anjum, M. R. Khan, and N. K. Janjua, “Electro□oxidation of ammonia over copper oxide impregnated γ□al2o3 nanocatalysts,” *Coatings*, vol. 11, no. 3, Mar. 2021, doi: 10.3390/coatings11030313.

[12] S. Khan, S. S. Shah, M. A. R. Anjum, M. R. Khan, and N. K. Janjua, “Electro□oxidation of ammonia over copper oxide impregnated γ□al2o3 nanocatalysts,” *Coatings*, vol. 11, no. 3, Mar. 2021, doi: 10.3390/coatings11030313.

[13] S. W. Wallace, I. T. McCrum, and M. J. Janik, “Ammonia electro-oxidation mechanism on the platinum (100) surface,” *Catal Today*, vol. 371, pp. 50–57, Jul. 2021, doi: 10.1016/J.CATTOD.2020.09.024.

[14] G. Jeerh, P. Zou, M. Zhang, S. Chen, J. Humphreys, and S. Tao, “Electrooxidation of ammonia on A-site deficient perovskite oxide La0.9Ni0.6Cu0.35Fe0.05O3-δ for wastewater treatment,” *Sep Purif Technol*, vol. 297, p. 121451, Sep. 2022, doi: 10.1016/J.SEPPUR.2022.121451.

[15] G. Jeerh, P. Zou, M. Zhang, and S. Tao, “Perovskite oxide LaCr0.25Fe0.25Co0.5O3-δ as an efficient non-noble cathode for direct ammonia fuel cells,” *Appl Catal B*, vol. 319, p. 121919, Dec. 2022, doi: 10.1016/J.APCATB.2022.121919.

[16] S. Johnston *et al.*, “A Survey of Catalytic Materials for Ammonia Electrooxidation to Nitrite and Nitrate,” *ChemSusChem*, vol. 15, no. 20, Oct. 2022, doi: 10.1002/cssc.202200614.

[17] U. Department of Energy, “Potential Roles of Ammonia in a Hydrogen Economy A Study of Issues Related to the Use Ammonia for On-Board Vehicular Hydrogen Storage,” 2006.

[18] J. Cai *et al.*, “Electrocatalytic nitrate-to-ammonia conversion with ~100% Faradaic efficiency via single-atom alloying,” *Appl Catal B*, vol. 316, p. 121683, Nov. 2022, doi: 10.1016/J.APCATB.2022.121683.

[19] J. Lee, S. Ga, D. Lim, S. Lee, H. Cho, and J. Kim, “Carbon-free green hydrogen production process with induction heating-based ammonia decomposition reactor,” *Chemical Engineering Journal*, p. 141203, Dec. 2022, doi: 10.1016/J.CEJ.2022.141203.

[20] Y. Xu *et al.*, “Engineering the surface chemical microenvironment over CuO nanowire arrays by polyaniline modification for efficient ammonia electrosynthesis from nitrate,” *Appl Catal B*, vol. 320, p. 121981, Jan. 2023, doi: 10.1016/J.APCATB.2022.121981.

[21] I. Lucentini, G. García Colli, C. D. Luzi, I. Serrano, O. M. Martínez, and J. Llorca, “Catalytic ammonia decomposition over Ni-Ru supported on CeO2 for hydrogen production: Effect of metal loading and kinetic analysis,” *Appl Catal B*, vol. 286, p. 119896, Jun. 2021, doi: 10.1016/J.APCATB.2021.119896.

[22] D. Ma, A. Hasanbeigi, L. Price, and W. Chen, “Assessment of energy-saving and emission reduction potentials in China’s ammonia industry,” *Clean Technol Environ Policy*, vol. 17, no. 6, pp. 1633–1644, Aug. 2015, doi: 10.1007/S10098-014-0896-3.

[23] F. Vitse, M. Cooper, and G. G. Botte, “On the use of ammonia electrolysis for hydrogen production,” *J Power Sources*, vol. 142, no. 1–2, pp. 18–26, Mar. 2005, doi: 10.1016/J.JPOWSOUR.2004.09.043.

[24] R. Chen *et al.*, “Performance of direct ammonia fuel cell with PtIr/C, PtRu/C, and Pt/C as anode electrocatalysts under mild conditions,” *Int J Hydrogen Energy*, vol. 46, no. 54, pp. 27749–27757, Aug. 2021, doi: 10.1016/j.ijhydene.2021.06.001.

[25] H. G. Oswin and M. Salo~rion~, “THE ANODIC OXIDATION OF AMMONIA AT PLATINUM BLACK ELECTRODES IN AQUEOUS KOH ELECTROLYTE.”

[26] H. Zhang *et al.*, “Sulfur induced surface reconfiguration of Ni1Cu3-S-T/CP anode for high-efficiency ammonia electro-oxidation,” *Chemical Engineering Journal*, vol. 452, Jan. 2023, doi: 10.1016/j.cej.2022.139582.

[27] N. J. Bunce and D. Bejan, “Mechanism of electrochemical oxidation of ammonia,” *Electrochim Acta*, vol. 56, no. 24, pp. 8085–8093, Oct. 2011, doi: 10.1016/J.ELECTACTA.2011.07.078.

[28] X. Xi *et al.*, “Carbon-free sustainable energy technology: Electrocatalytic ammonia oxidation reaction,” *Chemical Engineering Journal*, vol. 435, p. 134818, May 2022, doi: 10.1016/J.CEJ.2022.134818.

[29] C. Zhong, W. B. Hu, and Y. F. Cheng, “Recent advances in electrocatalysts for electro-oxidation of ammonia,” *J Mater Chem A Mater*, vol. 1, no. 10, pp. 3216–3238, Mar. 2013, doi: 10.1039/c2ta00607c.

[30] G. Soloveichik, “Electrochemical synthesis of ammonia as a potential alternative to the Haber–Bosch process,” *Nature Catalysis*, vol. 2, no. 5. Nature Publishing Group, pp. 377–380, May 01, 2019. doi: 10.1038/s41929-019-0280-0.

[31] Z.-H. Lyu, J. Fu, T. Tang, J. Zhang, and J.-S. Hu, “Design of ammonia oxidation electrocatalysts for efficient direct ammonia fuel cells,” *EnergyChem*, p. 100093, Dec. 2022, doi: 10.1016/J.ENCHEM.2022.100093.

[32] X. Jiang *et al.*, “Identification of the role of Cu site in Ni-Cu hydroxide for robust and high selective electrochemical ammonia oxidation to nitrite,” *Electrochim Acta*, vol. 345, Jun. 2020, doi: 10.1016/j.electacta.2020.136157.

[33] B. A. López De Mishima, D. Lescano, T. Molina Holgado, and H. T. Mishima, “Electrochemical oxidation of ammonia in alkaline solutions: its application to an

amperometric sensor," *Electrochim Acta*, vol. 43, no. 3–4, pp. 395–404, Jan. 1998, doi: 10.1016/S0013-4686(97)00061-3.

[34] Z. F. Li, Y. Wang, and G. G. Botte, "Revisiting the electrochemical oxidation of ammonia on carbon-supported metal nanoparticle catalysts," *Electrochim Acta*, vol. 228, pp. 351–360, Feb. 2017, doi: 10.1016/J.ELECTACTA.2017.01.020.

[35] K. Yao and Y. F. Cheng, "Electrodeposited Ni–Pt binary alloys as electrocatalysts for oxidation of ammonia," *J Power Sources*, vol. 173, no. 1, pp. 96–101, Nov. 2007, doi: 10.1016/J.JPOWSOUR.2007.04.081.

[36] T. L. Lomocso and E. A. Baranova, "Electrochemical oxidation of ammonia on carbon-supported bi-metallic PtM (M = Ir, Pd, SnOx) nanoparticles," *Electrochim Acta*, vol. 56, no. 24, pp. 8551–8558, Oct. 2011, doi: 10.1016/J.ELECTACTA.2011.07.041.

[37] C. M. Hung, "Electrochemical properties of PtPdRh alloy catalysts for ammonia electrocatalytic oxidation," *Int J Hydrogen Energy*, vol. 37, no. 18, pp. 13815–13821, Sep. 2012, doi: 10.1016/J.IJHYDENE.2012.03.147.

[38] K. Yao and Y. F. Cheng, "Investigation of the electrocatalytic activity of nickel for ammonia oxidation," *Mater Chem Phys*, vol. 108, no. 2–3, pp. 247–250, Apr. 2008, doi: 10.1016/j.matchemphys.2007.09.030.

[39] A. Kapałka, A. Cally, S. Neodo, C. Comninellis, M. Wächter, and K. M. Udert, "Electrochemical behavior of ammonia at Ni/Ni(OH)2 electrode," *Electrochem commun*, vol. 12, no. 1, pp. 18–21, Jan. 2010, doi: 10.1016/j.elecom.2009.10.026.

[40] L. Candido and J. A. C. P. Gomes, "Evaluation of anode materials for the electro-oxidation of ammonia and ammonium ions," *Mater Chem Phys*, vol. 129, no. 3, pp. 1146–1151, Oct. 2011, doi: 10.1016/j.matchemphys.2011.05.080.

[41] Y. J. Shih, Y. H. Huang, and C. P. Huang, "Electrocatalytic ammonia oxidation over a nickel foam electrode: Role of Ni(OH)2(s)-NiOOH(s) nanocatalysts," *Electrochim Acta*, vol. 263, pp. 261–271, Feb. 2018, doi: 10.1016/j.electacta.2018.01.045.

[42] Y. J. Shih, Y. H. Huang, and C. P. Huang, "Electrocatalytic ammonia oxidation over a nickel foam electrode: Role of Ni(OH)2(s)-NiOOH(s) nanocatalysts," *Electrochim Acta*, vol. 263, pp. 261–271, Feb. 2018, doi: 10.1016/j.electacta.2018.01.045.

[43] X. Li, J. Yu, and M. Jaroniec, "Hierarchical photocatalysts," *Chemical Society Reviews*, vol. 45, no. 9. Royal Society of Chemistry, pp. 2603–2636, May 07, 2016. doi: 10.1039/c5cs00838g.

[44] N. Shang *et al.*, "Constructing hierarchical structure electrocatalyst for efficient hydrogen evolution and selective oxidation of benzylamine," *J Alloys Compd*, vol. 912, p. 165259, Aug. 2022, doi: 10.1016/J.JALLCOM.2022.165259.

[45] N. Shang *et al.*, "Constructing hierarchical structure electrocatalyst for efficient hydrogen evolution and selective oxidation of benzylamine," *J Alloys Compd*, vol. 912, p. 165259, Aug. 2022, doi: 10.1016/J.JALLCOM.2022.165259.

[46] M. Fang *et al.*, "Hierarchical NiMo-based 3D electrocatalysts for highly-efficient hydrogen evolution in alkaline conditions," *Nano Energy*, vol. 27, pp. 247–254, Sep. 2016, doi: 10.1016/J.NANOEN.2016.07.005.

[47] Z. Sun, T. Liao, K. Liu, L. Jiang, J. H. Kim, and S. X. Dou, "Robust superhydrophobicity of hierarchical ZnO hollow microspheres fabricated by two-step self-assembly," *Nano Res*, vol. 6, no. 10, pp. 726–735, 2013, doi: 10.1007/s12274-013-0350-6.

[48] S. A. Chala *et al.*, "Hierarchical 3D Architectured Ag Nanowires Shelled with NiMn-Layered Double Hydroxide as an Efficient Bifunctional Oxygen Electrocatalyst," *ACS Nano*, vol. 14, no. 2, pp. 1770–1782, Feb. 2020, doi: 10.1021/acsnano.9b07487.

[49] B. Robert Viner Stanford, "CIII. NESSLERISATION, AND THE AVOIDANCE OF TURBIDITY IN NESSLERISED SOLUTIONS."

[50] W. Xu *et al.*, "Electrodeposited NiCu bimetal on carbon paper as stable non-noble anode for efficient electrooxidation of ammonia," *Appl Catal B*, pp. 1101–1109, Dec. 2018, doi: 10.1016/j.apcatb.2016.11.003.

[51] M. Kooti, M. Kooti, and L. Matouri, "Fabrication of Nanosized Cuprous Oxide Using Fehling's Solution," 2010. [Online]. Available: https://www.researchgate.net/publication/259323045

[52] T. Theivasanthi and M. Alagar, "X-Ray Diffraction Studies of Copper Nanopowder."

[53] Y. Li *et al.*, "β-Nickel hydroxide cathode material for nano-suspension redox flow batteries," *Frontiers in Energy*, vol. 11, no. 3, pp. 401–409, Sep. 2017, doi: 10.1007/s11708-017-0496-0.

[54] L. Chen *et al.*, "Fabrication of β-Ni(OH)2 Particles by Alkaline Etching Layered Double Hydroxides Precursor for Supercapacitor," *Front Energy Res*, vol. 9, Jan. 2022, doi: 10.3389/fenrg.2021.810568.

[55] Y. Xin *et al.*, "Stability-Enhanced α-Ni(OH)2Pillared by Metaborate Anions for Pseudocapacitors," *ACS Appl Mater Interfaces*, vol. 13, no. 24, pp. 28118–28128, Jun. 2021, doi: 10.1021/acsami.1c04525.

[56] C.-C. Yang, "Synthesis and characterization of active materials of Ni(OH) 2 powders," 2002. [Online]. Available: www.elsevier.com/locate/ijhydene

[57] J. Yu, S. Pan, Y. Zhang, Q. Liu, and B. Li, "Facile synthesis of monodispersed α-ni(oh)2 microspheres assembled by ultrathin nanosheets and its performance for oxygen evolution reduction," *Front Mater*, vol. 6, May 2019, doi: 10.3389/fmats.2019.00124.

[58] Q. Hu *et al.*, "Hollow Cu-doped NiO microspheres as anode materials with enhanced lithium storage performance," *RSC Adv*, vol. 9, no. 36, pp. 20963–20967, 2019, doi: 10.1039/c9ra03780b.

[59] J. T. Richardson, R. Scates, and M. V. Twigg, “X-ray diffraction study of nickel oxide reduction by hydrogen,” *Appl Catal A Gen*, vol. 246, no. 1, pp. 137–150, Jun. 2003, doi: 10.1016/S0926-860X(02)00669-5.

[60] X. Xu *et al.*, “Engineering Ni3+ Cations in NiO Lattice at the Atomic Level by Li+ Doping: The Roles of Ni3+ and Oxygen Species for CO Oxidation,” *ACS Catal*, vol. 8, no. 9, pp. 8033–8045, Sep. 2018, doi: 10.1021/acscatal.8b01692.

[61] M. Zhang *et al.*, “A symmetric direct ammonia fuel cell using ternary NiCuFe alloy embedded in a carbon network as electrodes,” *J Mater Chem A Mater*, vol. 10, no. 36, pp. 18701–18713, Aug. 2022, doi: 10.1039/d2ta04129d.

[62] R. Wang, H. Liu, K. Zhang, G. Zhang, H. Lan, and J. Qu, “Ni(II)/Ni(III) redox couple endows Ni foam-supported Ni2P with excellent capability for direct ammonia oxidation,” *Chemical Engineering Journal*, vol. 404, Jan. 2021, doi: 10.1016/j.cej.2020.126795.

[63] P. Dubey, N. Kaurav, R. S. Devan, G. S. Okram, and Y. K. Kuo, “The effect of stoichiometry on the structural, thermal and electronic properties of thermally decomposed nickel oxide,” *RSC Adv*, vol. 8, no. 11, pp. 5882–5890, 2018, doi: 10.1039/c8ra00157j.

[64] B. P. Payne, M. C. Biesinger, and N. S. McIntyre, “The study of polycrystalline nickel metal oxidation by water vapour,” *J Electron Spectros Relat Phenomena*, vol. 175, no. 1–3, pp. 55–65, Jan. 2009, doi: 10.1016/j.elspec.2009.07.006.

[65] S. Sundar, G. Venkatachalam, and S. J. Kwon, “Biosynthesis of copper oxide (Cuo) nanowires and their use for the electrochemical sensing of dopamine,” *Nanomaterials*, vol. 8, no. 10, Oct. 2018, doi: 10.3390/nano8100823.

[66] W. Xu *et al.*, “Directly growing hierarchical nickel-copper hydroxide nanowires on carbon fibre cloth for efficient electrooxidation of ammonia,” *Appl Catal B*, vol. 218, pp. 470–479, 2017, doi: 10.1016/j.apcatb.2017.07.005.

[67] H. Zhang *et al.*, "A core-shell NiCu@NiCuOOH 3D electrode induced by surface electrochemical reconstruction for the ammonia oxidation reaction," *Int J Hydrogen Energy*, vol. 47, no. 36, pp. 16080–16091, Apr. 2022, doi: 10.1016/j.ijhydene.2022.03.139.

[68] J. Huang, Z. Chen, J. Cai, Y. Jin, T. Wang, and J. Wang, "Activating copper oxide for stable electrocatalytic ammonia oxidation reaction via in-situ introducing oxygen vacancies," *Nano Res*, vol. 15, no. 7, pp. 5987–5994, Jul. 2022, doi: 10.1007/s12274-022-4279-5.

[69] S. Khan, S. S. Shah, M. A. R. Anjum, M. R. Khan, and N. K. Janjua, "Electro□oxidation of ammonia over copper oxide impregnated γ□al2o3 nanocatalysts," *Coatings*, vol. 11, no. 3, Mar. 2021, doi: 10.3390/coatings11030313.

[70] C. Di Dong, C. W. Chen, C. M. Kao, and C. M. Hung, "Synthesis, characterization, and application of CuO-modified TiO2 electrode exemplified for ammonia electro-oxidation," *Process Safety and Environmental Protection*, vol. 112, pp. 243–253, Nov. 2017, doi: 10.1016/J.PSEP.2017.05.016.

[71] A. Kapałka, A. Cally, S. Neodo, C. Comninellis, M. Wächter, and K. M. Udert, "Electrochemical behavior of ammonia at Ni/Ni(OH)2 electrode," *Electrochem commun*, vol. 12, no. 1, pp. 18–21, Jan. 2010, doi: 10.1016/j.elecom.2009.10.026.

[72] J. Huang, Z. Chen, J. Cai, Y. Jin, T. Wang, and J. Wang, "Activating copper oxide for stable electrocatalytic ammonia oxidation reaction via in-situ introducing oxygen vacancies," *Nano Res*, vol. 15, no. 7, pp. 5987–5994, Jul. 2022, doi: 10.1007/s12274-022-4279-5.

[73] E. Cossar, M. S. E. Houache, Z. Zhang, and E. A. Baranova, "Comparison of electrochemical active surface area methods for various nickel nanostructures," *Journal of Electroanalytical Chemistry*, vol. 870, Aug. 2020, doi: 10.1016/j.jelechem.2020.114246.

[74] K. Nagita, Y. Yuhara, K. Fujii, Y. Katayama, and M. Nakayama, “Ni- And Cu-co-Intercalated Layered Manganese Oxide for Highly Efficient Electro-Oxidation of Ammonia Selective to Nitrogen,” *ACS Appl Mater Interfaces*, vol. 13, no. 24, pp. 28098–28107, Jun. 2021, doi: 10.1021/acsami.1c04422.

[75] J. Huang, J. Cai, and J. Wang, “Nanostructured Wire-in-Plate Electrocatalyst for High-Durability Production of Hydrogen and Nitrogen from Alkaline Ammonia Solution,” *ACS Appl Energy Mater*, vol. 3, no. 5, pp. 4108–4113, May 2020, doi: 10.1021/acsaem.9b02545.

[76] Y. Guo, Z. Pan, and L. An, “Carbon-free sustainable energy technology: Direct ammonia fuel cells,” *J Power Sources*, vol. 476, p. 228454, Nov. 2020, doi: 10.1016/J.JPOWSOUR.2020.228454.

[77] Y. Li *et al.*, “Ternary PtIrNi Catalysts for Efficient Electrochemical Ammonia Oxidation,” *ACS Catal*, vol. 10, no. 7, pp. 3945–3957, Apr. 2020, doi: 10.1021/acscatal.9b04670.